University of New Mexico
UNM Digital Repository

Mechanical Engineering ETDs | Engineering ETDs

Fall 12-15-2018

# Stability of a Spinning Triangle Tethered Spacecraft System in a Circular Orbit

Matthew James Heitstuman

Follow this and additional works at: https://digitalrepository.unm.edu/me_etds

Part of the Mechanical Engineering Commons

Recommended Citation
Heitstuman, Matthew James. "Stability of a Spinning Triangle Tethered Spacecraft System in a Circular Orbit." (2018).
https://digitalrepository.unm.edu/me_etds/160

This Thesis is brought to you for free and open access by the Engineering ETDs at UNM Digital Repository. It has been accepted for inclusion in Mechanical Engineering ETDs by an authorized administrator of UNM Digital Repository. For more information, please contact disc@unm.edu.

Matthew James Heitstuman
*Candidate*

Mechanical Engineering
*Department*

This thesis is approved, and it is acceptable in quality and form for publication:

*Approved by the Thesis Committee:*

Professor Christopher Hall, Chairperson

Professor John Russell

Assistant Professor Sang Lee

**STABILITY OF A SPINNING TRIANGLE TETHERED**

**SPACECRAFT SYSTEM IN A CIRCULAR ORBIT**

**by**

**MATTHEW JAMES HEITSTUMAN**

**B.S., MECHANICAL ENGINEERING, 2011**

THESIS

Submitted in Partial Fulfillment of the
Requirements for the Degree of

**Master of Science**
**Mechanical Engineering**

The University of New Mexico
Albuquerque, New Mexico

**December, 2018**

**STABILITY OF A SPINNING TRIANGLE TETHERED SPACECRAFT SYSTEM IN A CIRCULAR ORBIT**

**by**

**Matthew James Heitstuman**

**B.S., Mechanical Engineering, University of Portland, 2011**

## ABSTRACT

Equations of motion are derived for a spinning triangle tethered spacecraft system and are used to analyze the stability of such systems. Floquet theory is applied to the linearized, periodic coefficient, equations of motion to analyze spin stability as a function of triangle geometry and the average spin rate of the satellite relative to the angular velocity of the spacecraft orbiting around a central body. The results of the Floquet analysis show that spin stability is achievable for many combinations of spacecraft geometry and spin rate. Spacecraft engineers or operators for a triangle-shaped tethered spacecraft can use this information for mission planning or design purposes.

## TABLE OF CONTENTS

## LIST OF FIGURES

## LIST OF TABLES

# Chapter 1

## Introduction

Tethered Satellite Systems (TSS) consist of a spacecraft connected by a long cable (i.e., space tether) to one or more rigid bodies – possibly other operational spacecraft – to form a single, interconnected, mechanical system. Numerous applications for TSS have been proposed over the years, many of which have flown in space. It is this body of knowledge, both experimental results and theoretical studies of TSS, upon which the work presented in this thesis builds to develop a model to analyze the spin stability of a triangular tethered spacecraft.

## Tethered Spacecraft Basics

Tethered satellite systems can be distinguished from their conventional spacecraft counterparts by three discriminating features: 1) size, 2) flexibility, and 3) ability to actively interact with the space environment, assuming an electrodynamic tether is used [1]. Historically, as described in NASA's *Tethers in Space Handbook*, the most common configuration of TSS has been the dumbbell [2]. The dumbbell configuration of a TSS is one in which two rigid bodies are connected to one another by a single tether. One example of a successful on-orbit TSS experiment is the Naval Research Laboratory's (NRL) Tether Physics and Survivability Experiment (TiPS). Figure 1 [3] shows TiPS in its deployed configuration. The tether length used in the mission was 4 km, which is not shown to scale in the figure. The objectives of this experiment were to: 1) enhance understanding of

librations, the pendulum-like motion of end masses about system center of mass, and 2) collect data on tether's susceptibility to damage by space debris [3].

Figure 1. Artist Portrayal of NRL's TiPS in Deployed Configuration

Over the years, researchers have found numerous applications for TSS. The first application for TSS was devised in the late 19th century [4]. Tsiolkovsky first proposed a space tether mission in his 1895 paper "Day-Dreams of Earth and Heaven". In that paper he described a spacecraft bound to a counterweight that is spun around its mass center to create artificial gravity. In the same paper, Tsiolkovsky also proposed the first momentum transfer maneuver between a TSS and another object in space. Additional tether applications include gravity stabilization for spacecraft in geosynchronous Earth orbit, orbit altitude maintenance using electrodynamic tethers in Earth orbit, tethered

constellation formation flying, or as part of a space elevator [5]. Applications associated with tethered spacecraft formation flying in a triangular configuration are the focus of this thesis.

## Objectives

The objective of this thesis is to build upon the previous work performed by Kim and Hall [6] to model rotating triangle tethered satellite systems for the proposed, but ultimately unfunded, NASA Submillimeter Probe of the Evolution of Cosmic Structure (SPECS) mission, and the work performed by Ellis and Hall [7] to model out-of-plane librations of spinning tethered satellite systems, which was an area of focus for Ellis' PhD dissertation [8]. Hughes's *Spacecraft Attitude Dynamics* book is also an important resource regarding the derivation of the equations for a spinning tri-inertial rigid body [9]. Motivation for this topic is to increase our understanding of the dynamics associated with the aforementioned triangular tethered satellite systems so that in the future, missions such as SPECS and The Sentinel [10] can become a reality.

# Chapter 2

## Review of Related Literature

This review of related literature presents a comprehensive overview of the work performed in the field of TSS, with particular focus on research related to stability of spinning TSS, and the associated analysis techniques.

### History of Tethered Spacecraft Research

As discussed in Chapter 1 under the Tethered Spacecraft Basics section, Tsiolkovsky was the first to propose use of tethers for space-based applications. In 1966, 70 years after Tsiolkovsky's original proposal, the first on-orbit tether experiment was conducted during the Gemini-XI mission. The experiment involved the deployment of a 30 meter tether by hand to demonstrate the creation of artificial gravity [11]. After the conclusion of the Gemini program, the next tether experiments were not conducted until the early 1990s. The Tethered Satellite System (TSS) set of Shuttle-based missions were a joint effort between NASA and the Italian Space Agency (ASI) that began in 1992 [2]. The TSS-1 mission launched in 1992 and successfully demonstrated over 20 hours of deployed gravity-gradient stabilized tether system before being reeled in [12], despite the ASI-provided satellite only deploying 268m above the Orbiter before jamming.

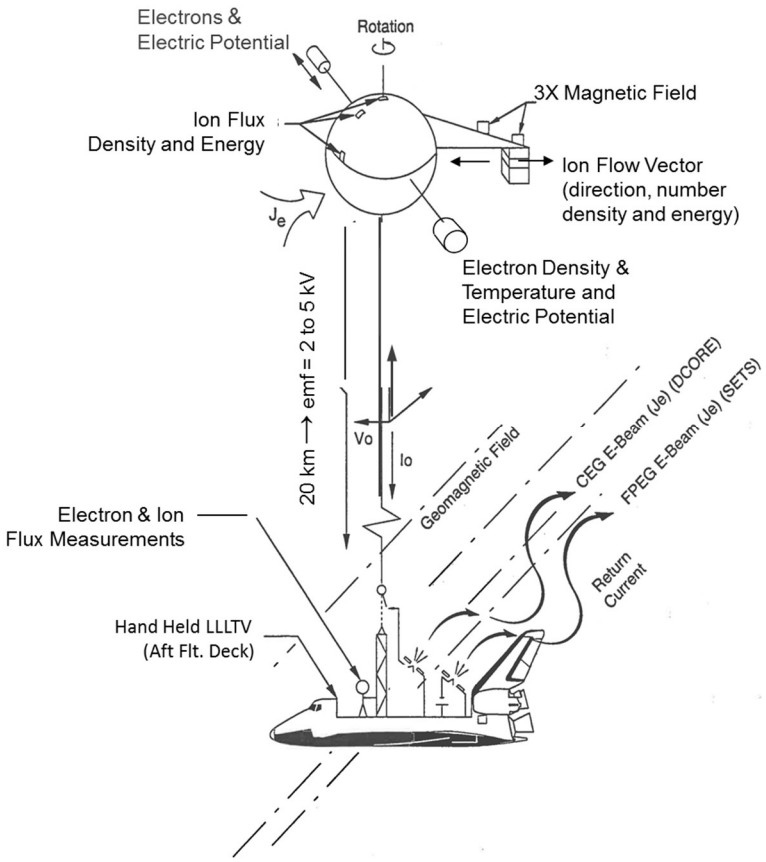


Figure 2. Functional Schematic of TSS-1

The TSS-1R mission launched in 1996 and built upon the results of TSS-1. The TSS-1R mission focused on exploring the electrodynamic properties of the tether that went untested during TSS-1. The TSS-1R mission ran into issues during deployment like TSS-1, but managed to deploy 19.7 km of tether. Fortunately, the length was sufficient to successfully demonstrate the electrodynamic properties of a conducting tether [2]. A functional schematic of TSS-1 is shown in Figure 2 [2].

The Small Expendable Deployer System (SEDS) project was the next attempt by NASA to study the deployment of tethers in space. The project consisted of two flights, SEDS-1

and SEDS-2, both of which launched as secondary payloads on Delta II launches of GPS satellites. The SEDS-1 and SEDS-2 experiments launched on 29 March 1993 and 9 March 1994, respectively. The primary mission objective of these experiments was to demonstrate the deployment of a payload using a 20 km-long tether. The same payload hardware was used for both flights of SEDS. The difference between the two missions was the implementation of open versus closed loop control on SEDS-1 and SEDS-2, respectively. Both missions successfully demonstrated the feasibility of the SEDS tether deployment mechanism. During SEDS-1, the velocity of the end-mass payload at the conclusion of deployment was calculated to be about 7 m/s using closed loop feedback to control the deployment mechanism. The use of closed loop feedback resulted in large jumps in tether tension as the end-mass payload rebounded in response to the abrupt stop, which could have ultimately caused the tether to fail. Fortunately, that did not occur. During SEDS-2, the tether deployment mechanism was able to carefully control the speed of deployment and was able to keep the final deployment velocity to about 2 cm/sec using closed loop feedback [2]. A SEDS-3 experiment was proposed for STS-85 to test a new deployment brake profile. However, the payload was de-manifested from STS-85 due to increasing schedule pressure to re-design the SEDS deployment safety components for the STS-85 mission [13]. The SEDS-3 experiment never launched.

The next tether experiment to launch was the NRL-developed TiPS on 20 June, 1996. As previously mentioned in Chapter 1, TiPS was a highly successful experiment exploring long-term tether survivability and on-orbit motion. The sponsor of the mission was the National Reconnaissance Office (NRO) and TiPS was the first unclassified, on-orbit

NRO-sponsored spacecraft [14]. The TiPS spacecraft was designed and built in about a year and leveraged mature, known designs – including the SEDS tether deployment mechanism [15]. Due to the secretive nature of the sponsor organization, very little information was published regarding the results of on-orbit experimentation. It was reported by NRL in 1999, however, that the mission was still operational [3] making it the longest operating known tether experiment.

Young Engineer Satellite-2 (YES2) was the latest successful on-orbit tethered spacecraft experiment conducted to date. YES2 is a 36 kg, student built experiment that piggybacked on the Russian-built Foton-M3 microgravity platform [16] deployed to Low Earth Orbit (LEO), as shown in Figure 3.

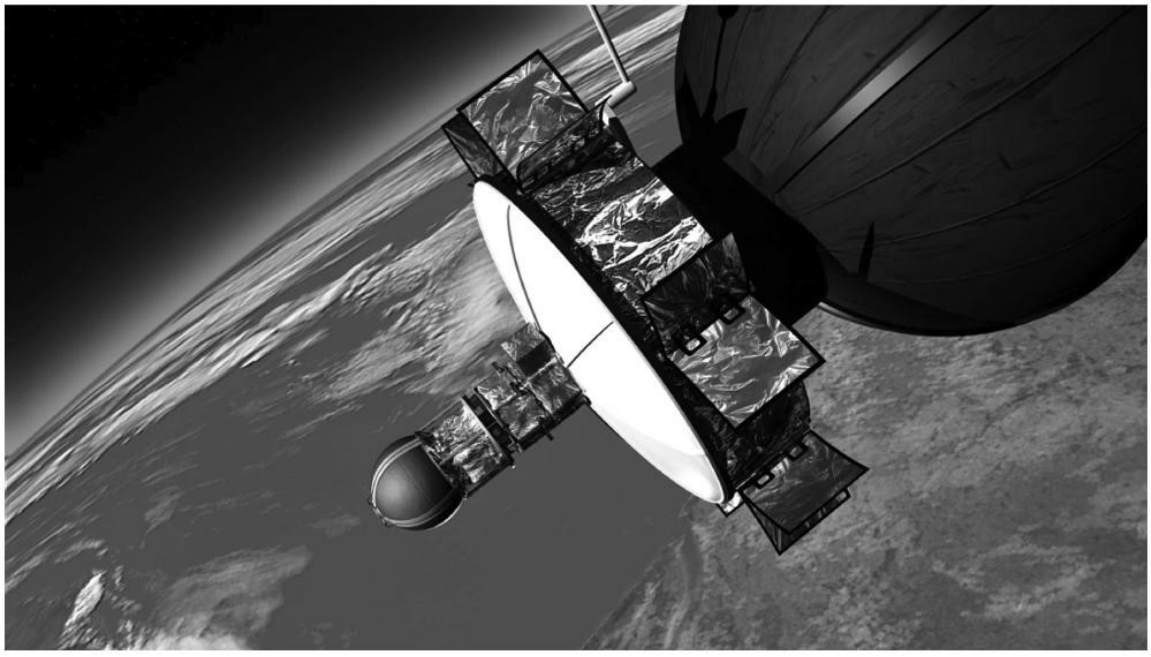

Figure 3. YES2 Attached to Foton-M3

The primary objective of the YES2 experiment was education for European college students and early-career engineers. Approximately 380 students were involved with the project over the life of the design and build of the experiment. The primary science objectives were "deployment of the 31.7 km tether in two stages to accurately release a 6 km spherical capsule [Fotino] into a reentry trajectory, and…landing of the capsule Fotino in Kazakhstan" [16]. The mission launched on 14 September 2007 and the YES2 experiment was switched on at 2:03:00 UTC on 25 September 2007. The tether deployed as expected, but there was a minor malfunction with the electronics on board causing a delay to the release of Fotino. Due to the release delay, Fotino is thought to have missed its anticipated landing zone by approximately 1250 km. It was never confirmed that Fotino landed successfully as it was never found. Nonetheless, the team declared success and claimed a world record for the longest deployed on-orbit tether [17].

In the years since the success of YES2 and TiPS, there have been no known successful on-orbit experiments involving TSS. Several tether missions have been proposed, such as the Propulsive SEDS (ProSEDS) mission and Momentum eXchange Electrodynamic Reboost (MXER). According to the final report published by NASA, the goal for ProSEDS, a proposed secondary payload on a Delta II launch of a GPS satellite like the original SEDS missions, was to "demonstrate high current collection by a bare tether to accelerate significantly the orbital decay of the Delta stage through the electrodynamic drag" [18]. The MXER mission, on the other hand, had the opposite goal of the ProSEDS mission. The goal of MXER was "Facility reboost…accomplished without propellant by driving current against a voltage created by a conducting tether's interaction with the

Earth's magnetic field (electrodynamic reboost). Uses for this system include transferring a variety of payloads (scientific, cargo, and human space vehicles) to multiple destinations including geosynchronous transfer orbit, the Moon or Mars" [19]. Both are fascinating applications of tether technology. Unfortunately, none of these missions made it past the concept phase of system development.

One aspect that all TSS missions flown to date share is the use of a single tether. It is possible to connect multiple bodies with tethers to create a formation of satellites and fly it as a single entity. In 2000, Quinn and Folta proposed using multiple tethers for the Sub-millimeter Probe of the Evolution of Cosmic Structure (SPECS) mission [20]. To accomplish the driving requirements for the SPECS mission, they proposed using a tethered formation of three 3-4 meter diameter mirrors connected to a central beam correlator in a triangle configuration, as shown in Figure 4 [20], to collect sub-millimeter photons.

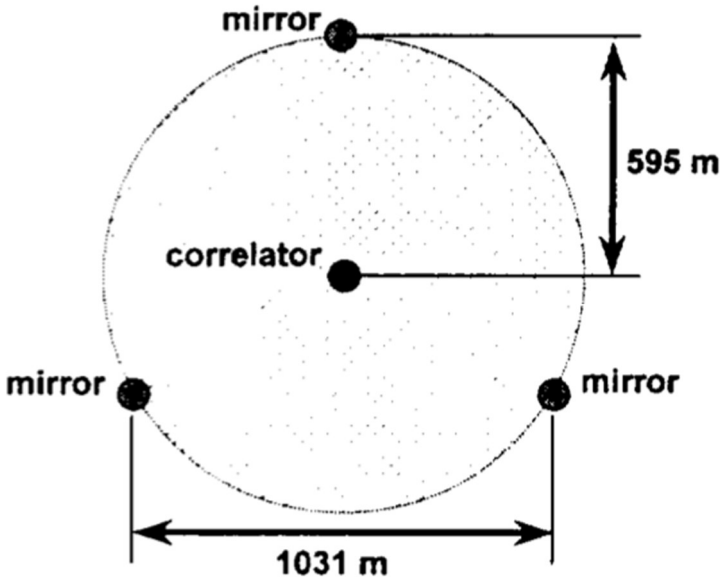


Figure 4. SPECS Design Concept for a 1 km Synthetic Aperture

They demonstrated the feasibility for their concept to perform the SPECS mission using a first order mathematical model of the proposed tethered formation. The authors recognized the need to further refine their mathematical model and for needed advancements in many technology areas, to include tether dynamics modeling, decentralized control methods, tether deployment mechanisms, tether material durability, and deployable booms. Several years after this concept was published, Kim and Hall proposed two alternate configurations for SPECS for which they developed system models and the motion equations [21]. The results of their work is considered in the creation of the triangle tether formation system model used in this thesis.

Another example of a proposed tether formation mission is the Sentinel CubeSat concept proposed by Timothy Berman while a graduate student at Virginia Polytechnic Institute

& State University. The Sentinel was proposed as an operationally responsive space mission with potential use cases for both the National Reconnaissance Office's intelligence collection mission and for civilian purposes [10]. The civilian concept of operations is to deploy the system in case of a natural disaster or terrorist attack to rapidly augment damaged ground telecommunications infrastructure. The same system also has the potential to intercept space-to-space communications on behalf of the Intelligence Community at large. Various orientations were proposed to accomplish the proposed Sentinel missions, shown below in the Figure 5.

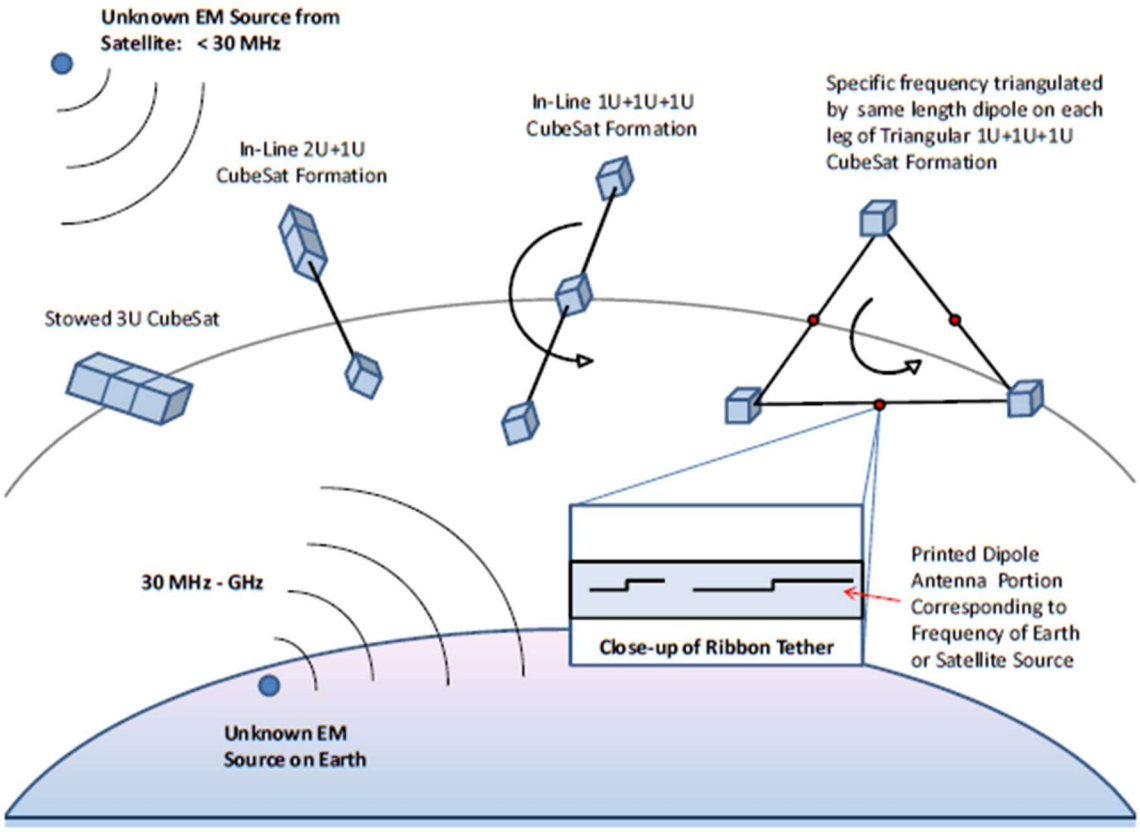


Figure 5. Proposed Formations and Orientations for The Sentinel

Berman attempted to determine the dynamics for the spinning triangular tether formation in his report. Unfortunately, his analysis of the problem led to an over-constrained system model and he was unable to define the equations of motion for a triangle TSS. When Berman simplified his equations, they became consistent with Ellis' mathematical model for the pendular motion of a tether spacecraft in a dumbbell configuration constrained to circular orbit [8]. Extending the dumbbell model to a triangular configuration is the focus of this thesis.

## Related Tether Dynamics Research

The work performed in this thesis builds upon the analysis performed by Dr. Ellis in his PhD dissertation [8] and the derivation of a spinning tri-inertial rigid body performed by Hughes [9]. Ellis explored modeling, dynamics, and control of spinning flexible TSS and his work built upon myriad research papers on spinning TSS. Chapter 3 of Ellis' work focused specifically on building a complete mathematical model of spinning flexible TSS and validating the results of the simplified models published in earlier research. Both the mathematical modeling and model validation are areas in which additional TSS research was needed [8]. Ellis performed a Floquet analysis to determine the stability of the spinning TSS used his mathematical model of a dumbbell TSS. The details of Floquet theory are presented in Chapter 3. Ellis used this analysis technique to determine the stability properties for a dumbbell TSS for various sets of initial conditions. Ellis' system model consisted of the following attributes, shown below in Figure 6: two end bodies connected by a single tether in orbit around a central body.

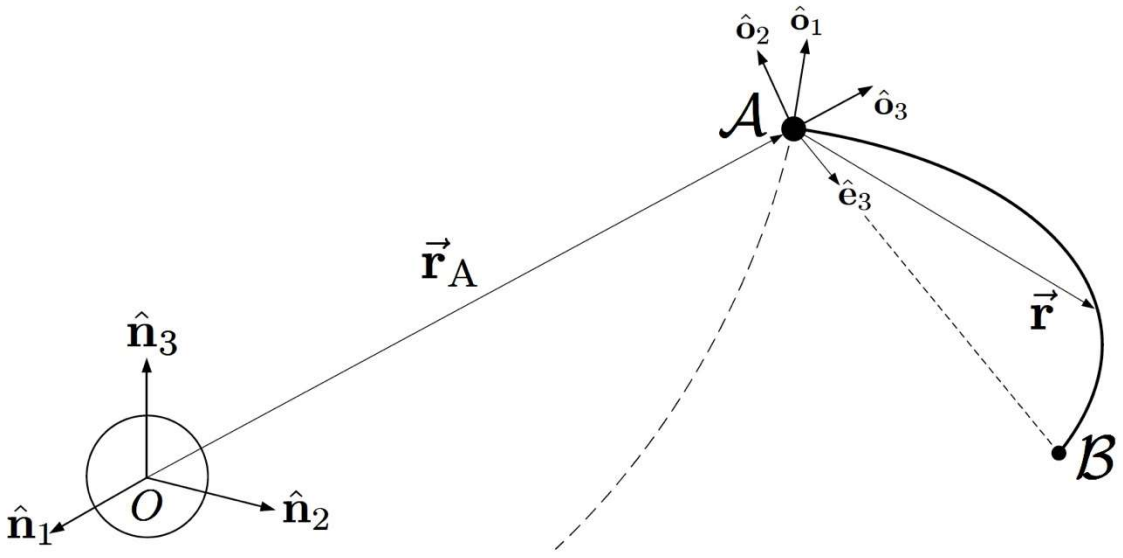


Figure 6. Low-Level System Model for Dumbbell TSS from Ellis' Dissertation

The analysis performed by Ellis made several assumptions that we leverage in this thesis. The assumptions are discussed in detail in a later chapter. Additionally, other researchers have derived the equations of motion for a triangle TSS, as well as performed a rudimentary stability analysis on their equations. Topal and Daybelge explored the tether dynamics of a triangle tethered satellite system in low earth orbit in 2005 [22]. Topal and Daybelge derived the equations of motion for the tether in a triangular tethered spacecraft system constrained to a circular orbit, which is of some use in this thesis. Hughes, in his book *Spacecraft Attitude Dynamics*, devoted an entire chapter to spinning rigid bodies in which he derives the equations of motion for a spinning tri-inertial rigid body [9]. He also proposed using Floquet theory to analyze the stability of the spinning rigid body. It is the goal of this thesis to build upon the work of Ellis and Hughes to determine the stability of a spinning triangle TSS.

# Chapter 3

## Methodology

This chapter covers assumptions, the development of the triangle TSS mathematical model, and the analysis performed to determine the conditions that cause the triangle TSS to become unstable.

### Assumptions

The following assumptions are made regarding the physical system and the environment in which the system resides. The physical system consists of three bodies connected by three tethers in orbit around a central body. The tethers are assumed to be non-conducting, thus the gravitational force is the only external force we will consider. The central body is assumed to be a spherical mass in which the density of the body is constant, thus the magnitude of the gravitational field is inversely proportional to the square of distance from the central body. Each of the three bodies are assumed to be point masses with equal mass. The tethers are treated as massless rigid rods, thus the entire system acts as a single rigid body. Finally, the triangular TSS is assumed constrained to an unperturbed circular orbit in the equatorial plane of the central body.

### System Model

First, we determine the coordinate frame and associated kinematics of the system to create a mathematical representation of the system. Figure 7 shows the configuration of the triangle TSS spinning around its center of mass.

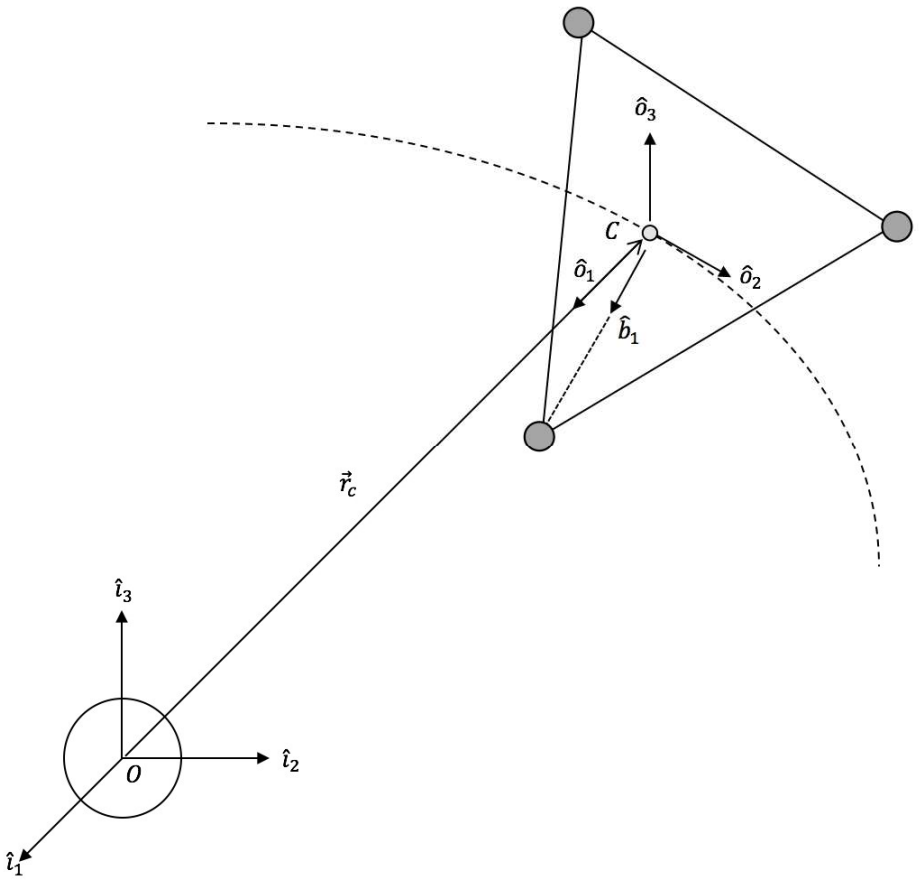


Figure 7. High-level Diagram of Spinning Triangle TSS Model

The inertial frame is centered at *O*, the center of the central body, and is denoted as $\mathcal{F}_i$ with coordinate axes $\hat{\imath}_n$. The orbital frame is centered at C, the centroid of the triangle TSS, and is denoted as $\mathcal{F}_o$ with coordinate axes $\hat{o}_n$. The triangle TSS is constrained to an unperturbed circular orbit, for which the equations of motion are known. Thus, the angular velocity of the TSS expressed in $\mathcal{F}_0$ relative to $\mathcal{F}_i$ is

$$\underset{\omega}{\rightarrow}_{oi} = \Omega_C \hat{o}_3 = [0 \quad 0 \quad \Omega_C]^T \tag{1}$$

with the magnitude of the angular velocity for a circular orbit is determined by:

$$\Omega_C = \sqrt{\mu / r_C^3} \tag{2}$$

where $\mu$ is the standard gravitation parameter of the central mass and $r_C$ is the distance from the center of the central mass to the centroid of the triangle TSS. Therefore, angular acceleration is zero because angular velocity is constant.

$$\dot{\underset{\omega}{\rightarrow}}_{oi} = 0 \tag{3}$$

Next, let $\mathcal{F}_b$ be defined as a body fixed coordinate frame with coordinate axes $\hat{b}_n$. The orbital frame $\mathcal{F}_o$ is transformed to $\mathcal{F}_b$ by performing a 3-2-1 Euler rotation sequence as shown in Figure 8. The 3-2-1 Euler rotation results in the rotation matrix shown in Equation 4, which is needed to define the angular velocity for the body frame relative to the orbital frame

$$R^{bo} = R_1(\gamma)R_2(\beta)R_3(\alpha) =$$

$$\begin{bmatrix} \mathrm{c}\,\alpha\,\mathrm{c}\,\beta & \mathrm{s}\,\alpha\,\mathrm{c}\,\beta & -\mathrm{s}\,\beta \\ -\mathrm{c}\,\gamma\,\mathrm{s}\,\alpha + \mathrm{c}\,\alpha\,\mathrm{s}\,\beta\,\mathrm{s}\,\gamma & \mathrm{c}\,\alpha\,\mathrm{c}\,\gamma + \mathrm{s}\,\alpha\,\mathrm{s}\,\beta\,\mathrm{s}\,\gamma & \mathrm{c}\,\beta\,\mathrm{s}\,\gamma \\ \mathrm{c}\,\alpha\,\mathrm{s}\,\beta\,\mathrm{c}\,\gamma + \mathrm{s}\,\alpha\,\mathrm{s}\,\gamma & \mathrm{s}\,\alpha\,\mathrm{s}\,\beta\,\mathrm{c}\,\gamma - \mathrm{c}\,\alpha\,\mathrm{s}\,\gamma & \mathrm{c}\,\beta\,\mathrm{c}\,\gamma \end{bmatrix} \tag{4}$$

where α is the in-plane angle and $\beta$ and $\gamma$ are the two out-of-plane angles. To find the angular velocity of $\mathcal{F}_b$ relative to $\mathcal{F}_o$ we follow the same process used to develop the rotation matrix in Equation 4. Following the 3-2-1 Euler rotation sequence once more, the angular velocity of $\mathcal{F}_b$ relative to $\mathcal{F}_o$ is:

$$\begin{aligned} \omega_{bo} &= \begin{bmatrix} \dot{\gamma} \\ 0 \\ 0 \end{bmatrix} + \begin{bmatrix} 1 & 0 & 0 \\ 0 & \mathrm{c}\,\gamma & \mathrm{s}\,\gamma \\ 0 & -\mathrm{s}\,\gamma & \mathrm{c}\,\gamma \end{bmatrix} \begin{bmatrix} 0 \\ \dot{\beta} \\ 0 \end{bmatrix} + \begin{bmatrix} 1 & 0 & 0 \\ 0 & \mathrm{c}\,\gamma & \mathrm{s}\,\gamma \\ 0 & -\mathrm{s}\,\gamma & \mathrm{c}\,\gamma \end{bmatrix} \begin{bmatrix} \mathrm{c}\,\beta & 0 & -\mathrm{s}\,\beta \\ 0 & 1 & 0 \\ \mathrm{s}\,\beta & 0 & \mathrm{c}\,\beta \end{bmatrix} \begin{bmatrix} 0 \\ 0 \\ \dot{\alpha} \end{bmatrix} \\ &= \begin{bmatrix} \dot{\gamma} - \mathrm{s}\,\beta\,\dot{\alpha} \\ \mathrm{c}\,\beta\,\mathrm{s}\,\gamma\,\dot{\alpha} + \mathrm{c}\,\gamma\,\dot{\beta} \\ \mathrm{c}\,\beta\,\mathrm{c}\,\gamma\,\dot{\alpha} - \mathrm{s}\,\gamma\,\dot{\beta} \end{bmatrix} \end{aligned} \tag{5}$$

Equation 5 defines the angular velocity of the triangular TSS as $\alpha$, $\beta$, and $\gamma$ evolve over time with respect to $\mathcal{F}_o$.

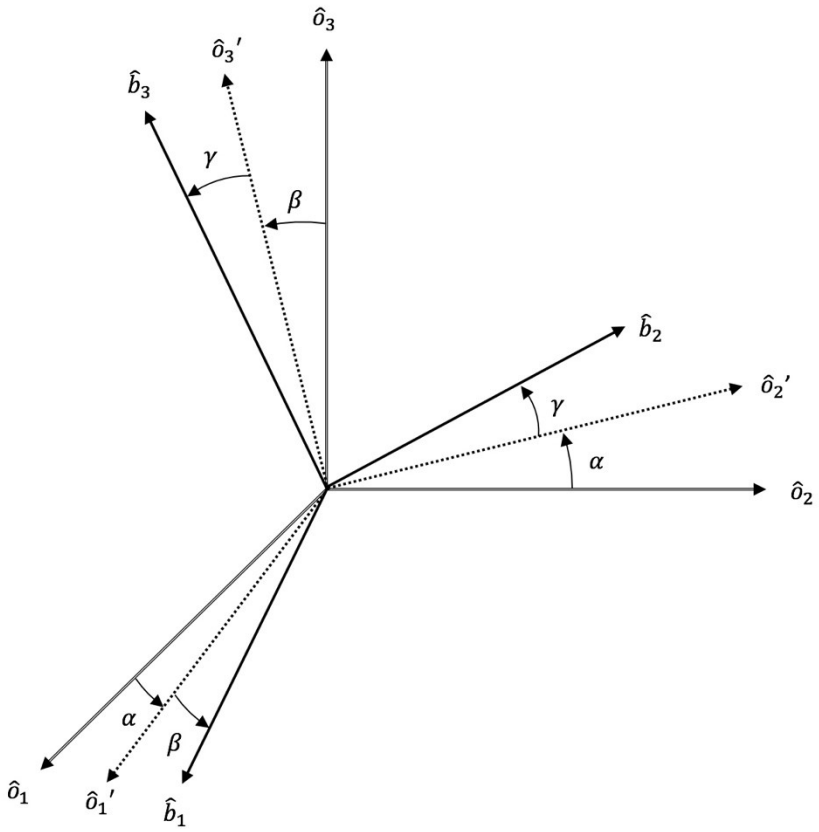


Figure 8. Orientation of $\mathcal{F}_b$ Relative to $\mathcal{F}_o$

The final step for determining the kinematics equations is to apply the angular momentum equations to the triangle TSS

$$\dot{\vec{h}} = \vec{g} \tag{6}$$

where $\dot{\vec{h}}$ is the time rate of change of angular momentum about the mass center and $\vec{g}$ is the torque about the mass center. For this analysis, we assume that gravity is the only force acting on the TSS. We can rewrite Equation 6 in body-frame components in matrix form as:

$$\dot{h} + \omega^{\times} h = g \tag{7}$$

Since $h = I\omega$, we can rewrite Equation 7 as

$$\dot{\omega} = -I^{-1}\omega^{\times} I\omega + I^{-1} g \tag{8}$$

where $I$ is the moment of inertia matrix and $\omega$ is the angular velocity of the body frame $\mathcal{F}_b$ with respect to the inertial frame $\mathcal{F}_i$. The relationship between $\omega_{bi}$ and $\omega_{bo}$ is governed by the rotation matrix previously calculated in Equation 4. We use $\omega_{bi}$ and $\omega_{bo}$ to determine the angular velocity of the spacecraft with respect to the inertial frame:

$$\omega_{bi} = \omega_{bo} + R^{bo}\omega_{oi} = \begin{bmatrix} \dot{\gamma} - \mathrm{s}\,\beta\,\dot{\alpha} \\ \mathrm{c}\,\beta\,\mathrm{s}\,\gamma\,\dot{\alpha} + \mathrm{c}\,\gamma\,\dot{\beta} \\ \mathrm{c}\,\beta\,\mathrm{c}\,\gamma\,\dot{\alpha} - \mathrm{s}\,\gamma\,\dot{\beta} \end{bmatrix} + \begin{bmatrix} -\mathrm{s}\,\beta\,\Omega_C \\ \mathrm{c}\,\beta\,\mathrm{s}\,\gamma\,\Omega_C \\ \mathrm{c}\,\beta\,\mathrm{c}\,\gamma\,\Omega_C \end{bmatrix} \tag{9}$$

$$\omega_{bi} = \begin{bmatrix} \dot{\gamma} - \mathrm{s}\,\beta\,(\dot{\alpha} + \Omega_C) \\ \mathrm{c}\,\gamma\,\dot{\beta} + \mathrm{c}\,\beta\,\mathrm{s}\,\gamma\,(\dot{\alpha} + \Omega_C) \\ -\mathrm{s}\,\gamma\,\dot{\beta} + \mathrm{c}\,\beta\,\mathrm{c}\,\gamma\,(\dot{\alpha} + \Omega_C) \end{bmatrix} \tag{10}$$

We have now determined the angular velocity equations for the triangle TSS. These equations are foundational to deriving the equations of motion for our triangle TSS. We can now determine the angular acceleration by differentiating $\omega_{bi}$:

$$\dot{\omega}_{bi} = \begin{bmatrix} \ddot{\gamma} - \mathrm{s}\,\beta\,\ddot{\alpha} - \mathrm{c}\,\beta\,\dot{\beta}(\dot{\alpha} + \Omega_C) \\ \mathrm{c}\,\beta\,\mathrm{s}\,\gamma\,\ddot{\alpha} - \mathrm{s}\,\gamma\,\dot{\beta}(\mathrm{s}\,\beta\,\dot{\alpha} + \mathrm{s}\,\beta\,\Omega_C + \dot{\gamma}) + \mathrm{c}\,\beta\,\mathrm{c}\,\gamma\,\dot{\gamma}(\dot{\alpha} + \Omega_C) + \mathrm{c}\,\gamma\,\ddot{\beta} \\ \mathrm{c}\,\beta\,\mathrm{c}\,\gamma\,\ddot{\alpha} - \mathrm{c}\,\gamma\,\dot{\beta}(\mathrm{s}\,\beta\,\dot{\alpha} + \mathrm{s}\,\beta\,\Omega_C + \dot{\gamma}) - \mathrm{c}\,\beta\,\mathrm{s}\,\gamma\,\dot{\gamma}(\dot{\alpha} + \Omega_C) - \mathrm{s}\,\gamma\,\ddot{\beta} \end{bmatrix} \tag{11}$$

The next step is to obtain an expression for the gravity gradient torque. This expression is needed in order to complete the series of pendular motion equations for the triangle TSS. The expression for the approximate gravity gradient torque around the mass center [23] using vector notation is:

$$g_g = 3\Omega_c^2 \hat{o}_1 \times \vec{I}_c \cdot \hat{o}_1 \tag{12}$$

Expressed in a body-fixed reference frame, the equation for gravity gradient torque is simplified to

$$g_g = 3\Omega_c^2 o_1^{\times} I o_1 \tag{13}$$

where $o_1$, as defined in Figure 7, is the nadir direction and the first column of the $R^{bo}$ rotation matrix; $o_1^{\times}$ is the skew-symmetric matrix of $o_1$; and $I$ is the moment of inertia about 'c' in $\mathcal{F}_b$ for the triangle TSS. The final equation needed to determine the pendular motion of the triangle TSS is the moment of inertia expressed in the body-fixed reference frame. Figure 9 shows the configuration of the triangle TSS used to compute the moment of inertia. The three bodies that constitute the triangle TSS are identified as T1, T2, and T3. T1 is aligned with $\hat{b}_1$, and T2 and T3 are both connected to T1 using tethers of equal length, defined as 'a' in Figure 9. The angle between the two tethers that are connected to T2 and T3 from T1 is defined as $\varphi$. The angle $\varphi$ is a key variable for determining the moment of inertia for the triangle TSS. Since we assume that two sides of the triangle that connect both T2 and T3 to T1 are of equal length, the configuration of the TSS is an isosceles triangle in all cases. In the case of $\varphi = 60°$, we have the special case of an equilateral triangle. This particular configuration of $\varphi = 60°$ simplifies our system to an axisymmetric rigid body. This special case is discussed further in Chapter 4.

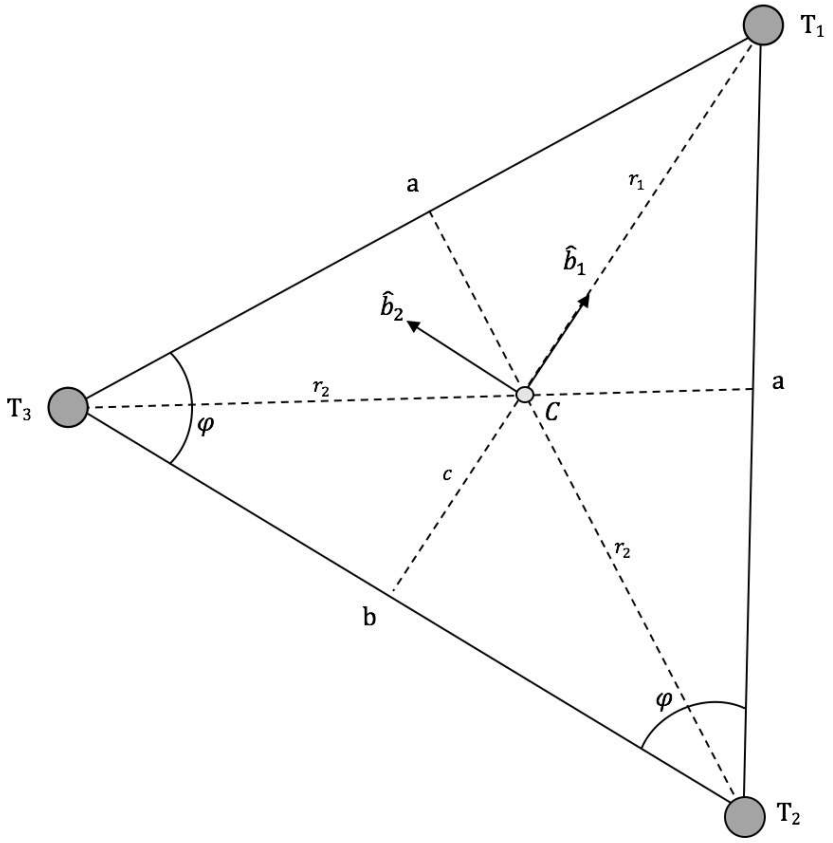


Figure 9. Configuration of Triangle Tethered Spacecraft System

The moment of inertia for the triangle TSS with each end body of equivalent mass ($m$) is

$$I_b^c = I_T = m\begin{bmatrix} b^2/2 & 0 & 0 \\ 0 & 2c^2 + {r_1}^2 & 0 \\ 0 & 0 & 2{r_2}^2 + {r_1}^2 \end{bmatrix} \tag{14}$$

where $b = 2a\cos\theta$, $c = b/2\tan(\theta/2)$, $r_1 = a\sin\theta - c$, and $r_2 = (b/2)/\cos(\theta/2)$. If, for example, we assume $a = 10$ km, $\varphi = 75°$ and $m = 1$ kg, we can reduce the moment of inertia for the triangle to the values in Equation 15. However, any values for $a$, $\varphi$, or $m$ are acceptable for analysis purposes.

$$I_T = \begin{bmatrix} 13.4 & 0 & 0 \\ 0 & 66.8 & 0 \\ 0 & 0 & 80.2 \end{bmatrix} = \begin{bmatrix} I_{T1} & 0 & 0 \\ 0 & I_{T2} & 0 \\ 0 & 0 & I_{T3} \end{bmatrix} \tag{15}$$

These resulting scalar values that constitute the moment of inertia of the triangle TSS satisfies Levin's formula for the moment of inertia for a two-dimensional triangle formation [24] ($I_{T1} + I_{T2} = I_{T3}$) and confirms we can classify the system as an asymmetric, also known as tri-inertial, rigid body. In the remainder of the derivation, we refer to the moment of inertia using $I_T$ from Equation 15. Now, we know from Equation 4 the values for $o_1$ and $o_1^{\times}$ as:

$$o_1 = \begin{bmatrix} \mathrm{c}\,\alpha\,\mathrm{c}\,\beta \\ -\mathrm{c}\,\gamma\,\mathrm{s}\,\alpha + \mathrm{c}\,\alpha\,\mathrm{s}\,\beta\,\mathrm{s}\,\gamma \\ \mathrm{c}\,\alpha\,\mathrm{s}\,\beta\,\mathrm{c}\,\gamma + \mathrm{s}\,\alpha\,\mathrm{s}\,\gamma \end{bmatrix} \tag{16}$$

$$o_1^{\times} = \begin{bmatrix} 0 & -(\mathrm{c}\,\alpha\,\mathrm{s}\,\beta\,\mathrm{c}\,\gamma + \mathrm{s}\,\alpha\,\mathrm{s}\,\gamma) & \mathrm{c}\,\gamma\,\mathrm{s}\,\alpha - \mathrm{c}\,\alpha\,\mathrm{s}\,\beta\,\mathrm{s}\,\gamma \\ \mathrm{c}\,\alpha\,\mathrm{s}\,\beta\,\mathrm{c}\,\gamma + \mathrm{s}\,\alpha\,\mathrm{s}\,\gamma & 0 & -\mathrm{c}\,\alpha\,\mathrm{c}\,\beta \\ -\mathrm{c}\,\gamma\,\mathrm{s}\,\alpha + \mathrm{c}\,\alpha\,\mathrm{s}\,\beta\,\mathrm{s}\,\gamma & \mathrm{c}\,\alpha\,\mathrm{c}\,\beta & 0 \end{bmatrix} \tag{17}$$

We can also rewrite Equation 13 in matrix form, using the principle moment of inertia calculated in Equation 15 as:

$$g_g = 3\Omega_c^2 \begin{bmatrix} (I_{T3} - I_{T2})o_{21}o_{31} \\ (I_{T1} - I_{T3})o_{11}o_{31} \\ (I_{T2} - I_{T1})o_{11}o_{21} \end{bmatrix} \tag{18}$$

Expanding Equation 6, expressed relative to $\mathcal{F}_b$, in matrix form and substituting the values from Equations 10, 11, 15, 16, and 17 will give us the governing equations for the pendular motion of the triangle TSS. We perform this substitution over the course of several steps. The first step to create the governing system of equations is to substitute the matrix equation for $g_g$ from Equation 18 into a rearranged version of Equation 6:

$$0 = I\dot{\omega} + \omega^{\times} I\omega - 3\Omega_c^2 \begin{bmatrix} (I_{T3} - I_{T2})o_{21}o_{31} \\ (I_{T1} - I_{T3})o_{11}o_{31} \\ (I_{T2} - I_{T1})o_{11}o_{21} \end{bmatrix} \tag{19}$$

The second step is to calculate the matrix form $I\dot{\omega}$ using Equation 15:

$$I\dot{\omega} = \begin{bmatrix} I_{T1} & 0 & 0 \\ 0 & I_{T2} & 0 \\ 0 & 0 & I_{T3} \end{bmatrix} \cdot \begin{bmatrix} \dot{\omega}_1 \\ \dot{\omega}_2 \\ \dot{\omega}_3 \end{bmatrix} = \begin{bmatrix} I_{T1}\dot{\omega}_1 \\ I_{T2}\dot{\omega}_2 \\ I_{T3}\dot{\omega}_3 \end{bmatrix} \tag{20}$$

The third step is to find $\omega^{\times} I\omega$ in matrix form using Equations 15:

$$\omega^{\times} I\omega = \begin{bmatrix} 0 & -\omega_3 & \omega_2 \\ \omega_3 & 0 & -\omega_1 \\ -\omega_2 & \omega_1 & 0 \end{bmatrix} \cdot \begin{bmatrix} I_{T1} & 0 & 0 \\ 0 & I_{T2} & 0 \\ 0 & 0 & I_{T3} \end{bmatrix} \cdot \begin{bmatrix} \omega_1 \\ \omega_2 \\ \omega_3 \end{bmatrix} = \begin{bmatrix} (I_{T3} - I_{T2})\omega_2\omega_3 \\ (I_{T1} - I_{T3})\omega_1\omega_3 \\ (I_{T2} - I_{T1})\omega_1\omega_2 \end{bmatrix} \tag{21}$$

Finally, we substitute the results from Equation 20 and Equation 21 into Equation 19:

$$0 = \begin{bmatrix} I_{T1}\dot{\omega}_1 \\ I_{T2}\dot{\omega}_2 \\ I_{T3}\dot{\omega}_3 \end{bmatrix} + \begin{bmatrix} (I_{T3} - I_{T2})\omega_2\omega_3 \\ (I_{T1} - I_{T3})\omega_1\omega_3 \\ (I_{T2} - I_{T1})\omega_1\omega_2 \end{bmatrix} - 3\Omega_c^2 \begin{bmatrix} (I_{T3} - I_{T2})o_{21}o_{31} \\ (I_{T1} - I_{T3})o_{11}o_{31} \\ (I_{T2} - I_{T1})o_{11}o_{21} \end{bmatrix} \tag{22}$$

Equation 22 is the general form of the equations of motion for an asymmetric rigid body, which applies to our triangle TSS. One of the observations that we can make looking at Equation 22 is that the individual magnitudes of the moment of inertia does not govern the motion of the triangle TSS. Only the ratios of the moment of inertia matter. Therefore, we can simplify the equations by establishing three ratios for the moment of inertia:

$$k_1 = \frac{(I_{T3} - I_{T1})}{I_{T2}} \tag{23}$$

$$k_2 = \frac{(I_{T2} - I_{T1})}{I_{T3}} \tag{24}$$

$$k_3 = \frac{(I_{T3} - I_{T2})}{I_{T1}} \tag{25}$$

These ratios allow us to further simplify the governing equations of motion in Equation 22 to the following:

$$\dot{\omega}_1 = -k_3[\omega_2\omega_3 - 3\Omega_c o_{21} o_{31}] \tag{26}$$

$$\dot{\omega}_2 = \quad k_1[\omega_1\omega_3 - 3\Omega_c o_{11} o_{31}] \tag{27}$$

$$\dot{\omega}_3 = -k_2[\omega_1\omega_2 - 3\Omega_c o_{11} o_{21}] \tag{28}$$

We can now substitute Equation 11 into Equations 26-28 to get the full set of governing motion equation for the triangle TSS in a circular orbit subject to gravity gradient torque. The equations for $o$ and are $\omega$ not included, but are located above in Equations 10 and 16, respectively:

$$\ddot{\gamma} = \mathrm{s}\,\beta\,\ddot{\alpha} + \mathrm{c}\,\beta\,\dot{\beta}(\dot{\alpha} + \Omega_C) - k_3[\omega_2\omega_3 - 3\Omega_c o_{21} o_{31}] \tag{29}$$

$$\begin{aligned}\ddot{\beta} = \mathrm{s}\,\gamma\Big[\Big(-\mathrm{c}\,\gamma\,\dot{\beta}(\mathrm{s}\,\beta\,\dot{\alpha} + \mathrm{s}\,\beta\,\Omega_C + \dot{\gamma}) - \mathrm{c}\,\beta\,\mathrm{s}\,\gamma\,\dot{\gamma}(\dot{\alpha} + \Omega_C)\Big) + \\ k_2[\omega_1\omega_2 - 3\Omega_c o_{11} o_{21}]\Big] - \\ \mathrm{c}\,\gamma\Big[\Big(-\mathrm{s}\,\gamma\,\dot{\beta}(\mathrm{s}\,\beta\,\dot{\alpha} + \mathrm{s}\,\beta\,\Omega_C + \dot{\gamma}) + \mathrm{c}\,\beta\,\mathrm{c}\,\gamma\,\dot{\gamma}(\dot{\alpha} + \Omega_C)\Big) - \\ k_1[\omega_1\omega_3 - 3\Omega_c o_{11} o_{31}]\Big]\end{aligned} \tag{30}$$

$$\begin{aligned}\ddot{\alpha} = (\mathrm{c}\,\beta\,\mathrm{c}\,\gamma)^{-1}\Big[-k_2[\omega_1\omega_2 - 3\Omega_c o_{11} o_{21}] + \mathrm{s}\,\gamma\,\ddot{\beta} - \\ \Big(-\mathrm{c}\,\gamma\,\dot{\beta}(\mathrm{s}\,\beta\,\dot{\alpha} + \mathrm{s}\,\beta\,\Omega_C + \dot{\gamma}) - \mathrm{c}\,\beta\,\mathrm{s}\,\gamma\,\dot{\gamma}(\dot{\alpha} + \Omega_C)\Big)\Big]\end{aligned} \tag{31}$$

The resulting equations of motion are a series of three nonlinear second-order differential equations. We are interested in determining the stability of the spin about the axis perpendicular to the plane of the system (i.e., $\alpha$). To determine stability about $\alpha$, we first solve the nonlinear equations using two sets of representative initial conditions that show stable and unstable motion, respectively. This allows us to determine the point at which

we linearize the equations of motion so we can perform a stability analysis of the in-plane motion. The initial conditions for the stable case are shown in Table 1.

Table 1. Initial Conditions for Nonlinear Equations of Motion: Stable Case

| ***Variable*** | ***Value(s)*** |
|---|---|
| $\varphi$ | $70°$ |
| $m$ | $1\ kg$ |
| $a$ | $10\ km$ |
| $r_c$ | $7000\ km$ |
| $\mu$ | $3.986 \times 10^5\ \ km^2/s^2$ |
| $\alpha_o$ | $0$ rad |
| $\beta_o$ | $0$ rad |
| $\gamma_o$ | $0$ rad |
| $\dot{\alpha}_0$ | $0$ (rad/s) |
| $\dot{\beta}_0$ | $1 \times 10^{-6}$ (rad/s) |
| $\dot{\gamma}_0$ | $1 \times 10^{-6}$ (rad/s) |

The results for the motion of the triangle TSS using the nonlinear equations are shown below in Figure 10.

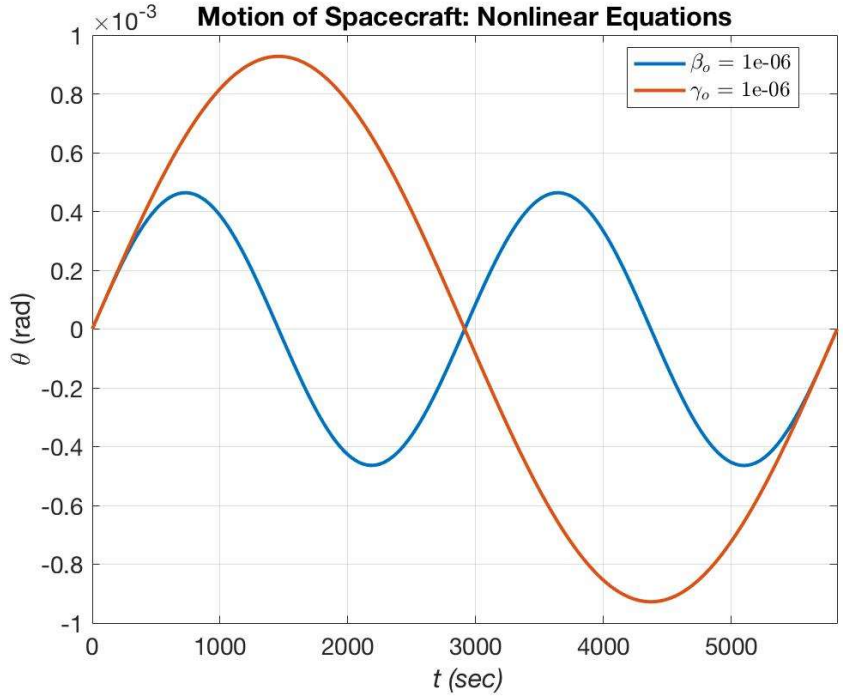


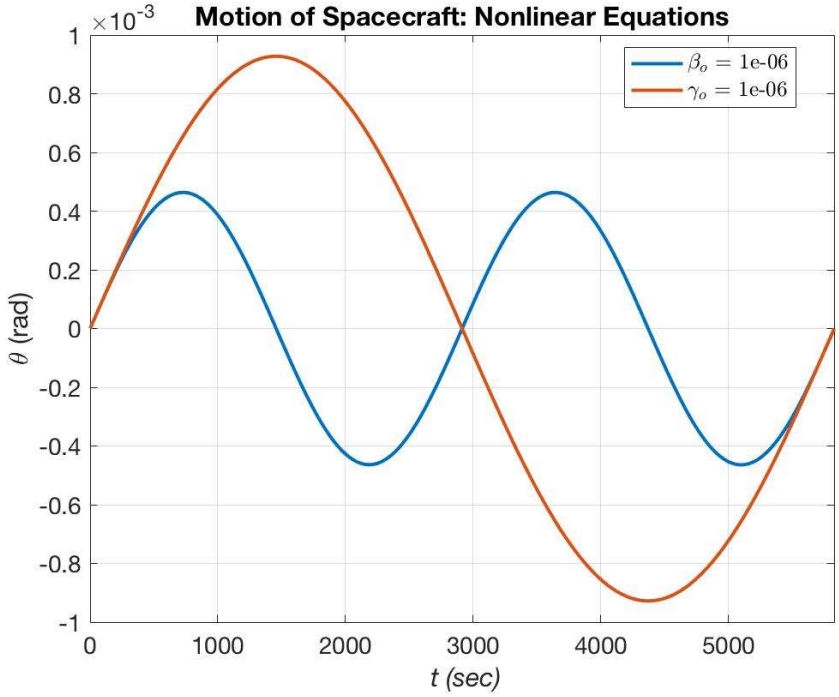


Figure 10. Numerical Solution of Nonlinear TSS Motion Equations: Stable Case

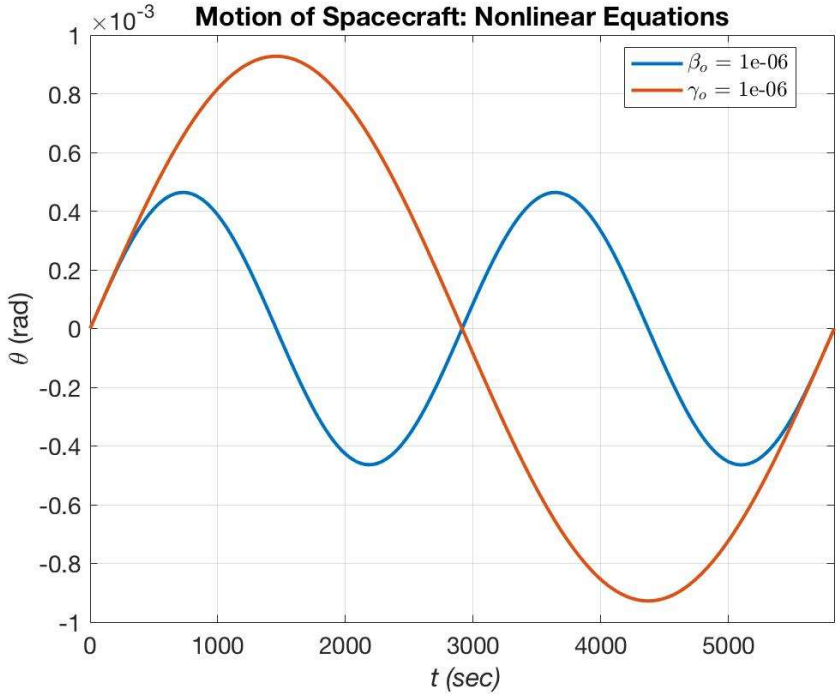


Figure 10 shows that the TSS motion remains stable over the course of the orbital period, which makes the initial conditions for $\beta$ and $\gamma$ candidates for linearization. Next, we solve the nonlinear equations of motion using initial conditions in Table 2 that cause unstable motion in our triangle TSS.

Table 2. Initial Conditions for Nonlinear Equations of Motion: Unstable

| *Variable* | *Value(s)* |
|---|---|
| $\varphi$ | $70°$ |
| $m$ | $1\ kg$ |
| $a$ | $10\ km$ |
| $r_c$ | $7000\ km$ |
| $\mu$ | $3.986 \times 10^5\ \ km^2/s^2$ |
| $\alpha_o$ | $0$ rad |
| $\beta_o$ | $0$ rad |
| $\gamma_o$ | $0$ rad |
| $\dot{\alpha}_0$ | $-\Omega_c$ (rad/s) |
| $\dot{\beta}_0$ | $\Omega_c/10$ (rad/s) |
| $\dot{\gamma}_0$ | $\Omega_c/10$ (rad/s) |

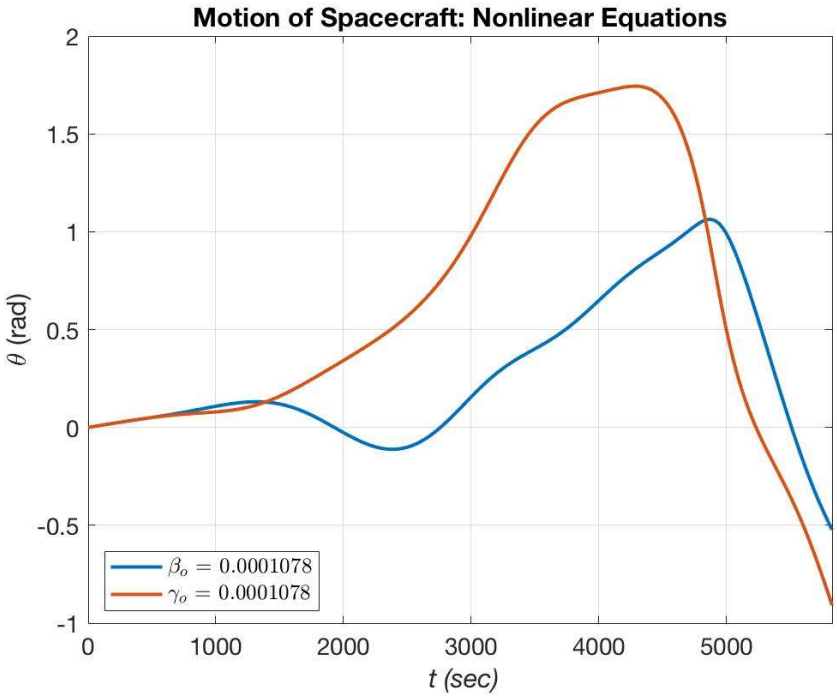


Figure 11. Numerical Solution of Nonlinear TSS Motion Equations: Unstable Case

We now need to linearize the equations of motion about known steady motion to perform the stability analysis for $\alpha$. We assume small $\beta$ and $\gamma$ (i.e., $\approx 0°$), which simplifies the nonlinear equations of motion for the triangle TSS to the following form:

$$\ddot{\gamma} = \beta\ddot{\alpha} + \dot{\beta}(\dot{\alpha} + \Omega_C) - k_3\left[\left(\dot{\beta} + \gamma(\dot{\alpha} + \Omega_C)\right)(\dot{\alpha} + \Omega_C) + 3\Omega_c^2(\mathrm{s}\,\alpha)(\mathrm{c}\,\alpha\,\beta + \mathrm{s}\,\alpha\,\gamma)\right] \tag{32}$$

$$\ddot{\beta} = -\gamma\ddot{\alpha} - \dot{\gamma}(\dot{\alpha} + \Omega_C) + k_1\left[\left(\dot{\gamma} - \beta(\dot{\alpha} + \Omega_C)\right)(\dot{\alpha} + \Omega_C) - 3\Omega_c^2(\mathrm{c}\,\alpha)(\mathrm{c}\,\alpha\,\beta + \mathrm{s}\,\alpha\,\gamma)\right] \tag{33}$$

$$\ddot{\alpha} = -k_2\left[\left(\dot{\gamma} - \beta(\dot{\alpha} + \Omega_C)\right)\left(\dot{\beta} + \gamma(\dot{\alpha} + \Omega_C)\right) + 3\Omega_c^2\,\mathrm{c}\,\alpha\,\mathrm{s}\,\alpha\right] \tag{34}$$

One additional step we can take to further simplify the equations is to define an "absolute pitch rate" as $\dot{\psi} = \dot{\alpha} + \Omega_C$ and substitute it into Equations 32-34:

$$\ddot{\gamma} = \beta\ddot{\alpha} + \dot{\beta}\dot{\psi} - k_3\left[\dot{\beta}\dot{\psi} + \gamma\dot{\psi}^2 + 3\Omega_c^2(\mathrm{s}\,\alpha)(\mathrm{c}\,\alpha\,\beta + \mathrm{s}\,\alpha\,\gamma)\right] \tag{35}$$

$$\ddot{\beta} = -\gamma\ddot{\alpha} - \dot{\gamma}\dot{\psi} + k_1\left[\dot{\gamma}\dot{\psi} - \beta\dot{\psi}^2 - 3\Omega_c^2(\mathrm{c}\,\alpha)(\mathrm{c}\,\alpha\,\beta + \mathrm{s}\,\alpha\,\gamma)\right] \tag{36}$$

$$\ddot{\alpha} = -k_2 3\Omega_c^2\,\mathrm{c}\,\alpha\,\mathrm{s}\,\alpha \tag{37}$$

We now need to linearize Equations 35 and 36 around our steady motion case of $\dot{\beta} = \beta = 0$ and $\dot{\gamma} = \gamma = 0$ in order to conduct the stability analysis. After linearization, we end up with the following equations of motion for $\ddot{\gamma}$ and $\ddot{\beta}$:

$$\ddot{\gamma} = (1 - k_3)\dot{\psi}\dot{\beta} + (\ddot{\alpha} - k_3 3\Omega_c^2\,\mathrm{c}\,\alpha\,\mathrm{s}\,\alpha)\beta - k_3\left(\dot{\psi}^2 + 3\Omega_c^2\,\mathrm{s}^2\,\alpha\right)\gamma \tag{38}$$

$$\ddot{\beta} = -(1 - k_1)\dot{\psi}\dot{\gamma} - k_1\left(\dot{\psi}^2 + 3\Omega_c^2\,\mathrm{c}^2\,\alpha\right)\beta - (\ddot{\alpha} + k_1 3\Omega_c^2\,\mathrm{c}\,\alpha\,\mathrm{s}\,\alpha)\gamma \tag{39}$$

Substituting Equation 37 into Equation 38 and 39 eliminates the $\ddot{\alpha}$ term, leading to the final form of the linear motion equations:

$$\ddot{\gamma} = (1 - k_3)\dot{\psi}\dot{\beta} - \left((k_2 + k_3)3\Omega_c^2 \, \mathrm{c}\,\alpha \, \mathrm{s}\,\alpha\right)\beta - k_3\left(\dot{\psi}^2 + 3\Omega_c^2 \, \mathrm{s}^2\,\alpha\right)\gamma \tag{40}$$

$$\ddot{\beta} = -(1 - k_1)\dot{\psi}\dot{\gamma} - k_1\left(\dot{\psi}^2 + 3\Omega_c^2 \, \mathrm{c}^2\,\alpha\right)\beta + \left((k_2 - k_1)3\Omega_c^2 \, \mathrm{c}\,\alpha \, \mathrm{s}\,\alpha\right)\gamma \tag{41}$$

We have now derived a set of linear equations that describe the motion for the spinning triangle TSS. These equations are equivalent to the equations derived by Hughes for a tri-inertial rigid satellite in a circular orbit [9]. In the following section, we will analyze the energy of the system to determine an equation for $\alpha$; solve our linear equations of motion for $\alpha$, $\beta$ and $\gamma$; and apply relevant elements of stability theory to Equations 40 and 41 to determine the stability properties of the triangle TSS.

## Analysis

This section covers several example solutions to the linear equations of motion and performs a Floquet analysis on the linear periodic-coefficient equations of motion to determine the stability properties of triangle TSS. Previous research performed on spinning dumbbell TSS determined that for small out-of-plane motion, the in-plane motion was not affected [8]. This relationship was leveraged by Ellis, who calculated the exact solution for the in-plane motion (i.e., $\hat{b}_2$– $\hat{b}_3$) and used that solution to develop the set of equations that govern the out-of-plane (i.e., $\hat{b}_1$– $\hat{b}_2$ and $\hat{b}_1$– $\hat{b}_3$) motion for a dumbbell TSS. We also need to find a solution to the in-plane motion equation ($\ddot{\alpha}$), which is needed for the numerical integration of Equations 40 and 41. As we show, the resulting solution for $\alpha$ is expressed in terms of periodic elliptic functions. Thus, we can apply Floquet theory to the system of homogenous linear equations with periodic coefficients to determine the stability properties of the out-of-plane motion of the TSS for various system configurations.

We start the analysis by solving the linear equations of motion for several triangle TSS configurations and visualizing the results over one orbital period. The initial conditions for the first test case are shown in Table 3:

Table 3. Initial Conditions for Linear Equations of Motion: Test Case 1

| ***Variable*** | ***Value(s)*** |
|---|---|
| $\varphi$ | $70°$ |
| $m$ | $1\ kg$ |
| $a$ | $10\ km$ |
| $r_c$ | $7000\ km$ |
| $\mu$ | $3.986 \times 10^5\ \ km^2/s^2$ |
| $\alpha_o$ | 0 rad |
| $\beta_o$ | 0 rad |
| $\gamma_o$ | 0 rad |
| $\dot{\alpha}_0$ | $0, 2\Omega_c, -\Omega_c$ (rad/s) |
| $\dot{\beta}_0$ | $1 \times 10^{-6}$ (rad/s) |
| $\dot{\gamma}_0$ | $1 \times 10^{-6}$ (rad/s) |

The equations are solved for several different values of $\dot{\alpha}_0$, which show how the TSS motion evolves over the orbital period. This variable $\theta$ is used in the following figures to indicate the angle between the triangle TSS in the body frame and the orbital frame. Runs one and three are repeats of the nonlinear cases we ran above. The results of the three runs at $\dot{\alpha}_0 = 0$, $\dot{\alpha}_0 = 2\Omega_c$ , and $\dot{\alpha}_0 = -\Omega_c$ are shown below in Figure 12, Figure 13, and Figure 14, respectively:

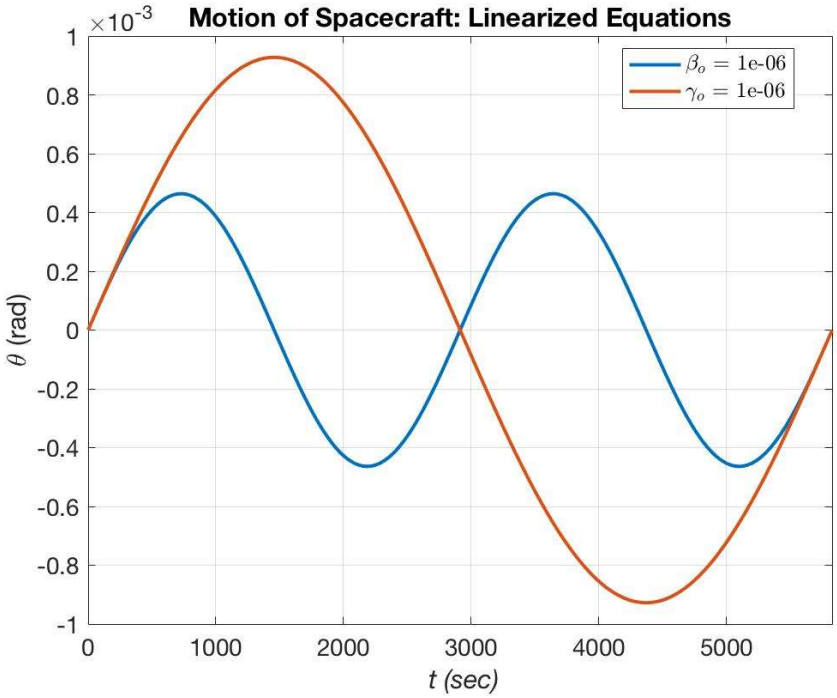


Figure 12. Numerical Solution to Motion Equations: $\varphi = 70°$, $\dot{\alpha}_0 = 0$

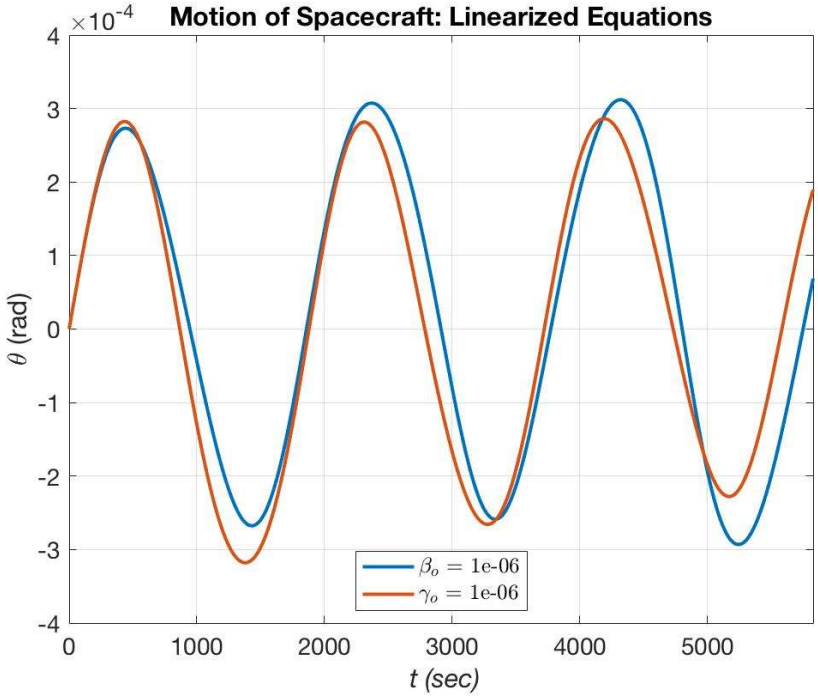


Figure 13. Numerical Solution to Motion Equations: $\varphi = 70°$, $\dot{\alpha}_0 = 2\Omega_c$

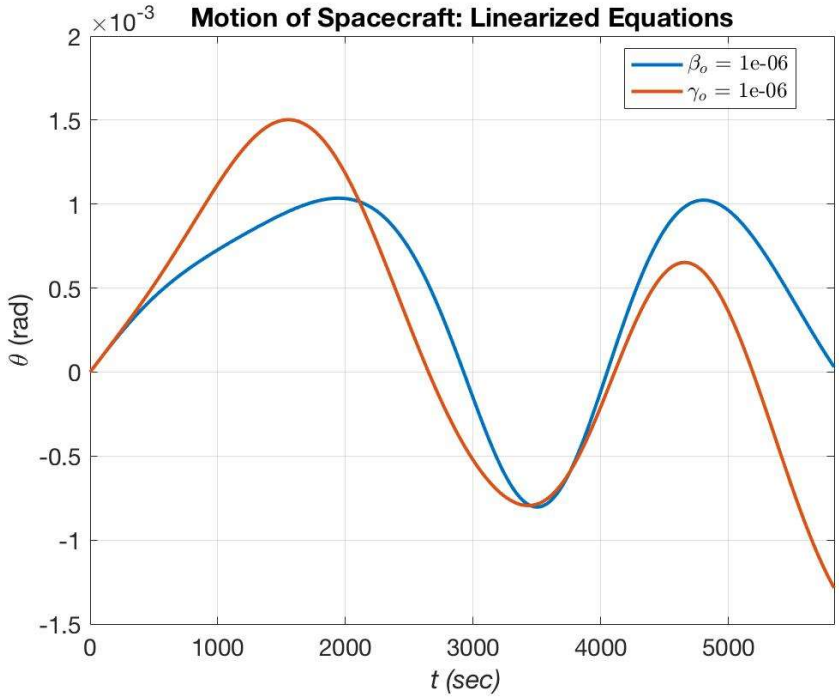


Figure 14. Numerical Solution to Motion Equations: $\varphi = 70°$, $\dot{\alpha}_0 = -\Omega_c$

It appears at first glance that the results of the numerical integration for the first two runs show stable TSS motion. It is worth noting that the results for run one are identical to the solution using the nonlinear equations, which is expected. The results for the third run appears to show unstable motion of the TSS. Run three is the same case that we solved above using the nonlinear version of the motion equations, which was also unstable. We conclude that the stability properties of the linearized equations are consistent thus far with the nonlinear equations. We now choose a different $\varphi$ for the second test case and solve the motion equations. The initial conditions for the second test case are shown in Table 4. We run the numerical integration for three values of $\dot{\alpha}_0$, as in the first test case, and investigate the stability of the TSS motion.

Table 4. Initial Conditions for Linear Equations of Motion: Test Case 2

| *Variable* | *Value(s)* |
|---|---|
| $\varphi$ | $85°$ |
| $m$ | $1\ kg$ |
| $a$ | $10\ km$ |
| $r_c$ | $7000\ km$ |
| $\mu$ | $3.986 \times 10^5\ \ km^2/s^2$ |
| $\alpha_o$ | 0 rad |
| $\beta_o$ | 0 rad |
| $\gamma_o$ | 0 rad |
| $\dot{\alpha}_0$ | $0, 2\Omega_c, -\Omega_c$ (rad/s) |
| $\dot{\beta}_0$ | $1 \times 10^{-6}$(rad/s) |
| $\dot{\gamma}_0$ | $1 \times 10^{-6}$(rad/s) |

The results of the three runs for the second test case at $\dot{\alpha}_0 = 0$, $\dot{\alpha}_0 = 2\Omega_c$ , and $\dot{\alpha}_0 = -\Omega_c$ are shown below in Figure 15, Figure 16, and Figure 17, respectively:

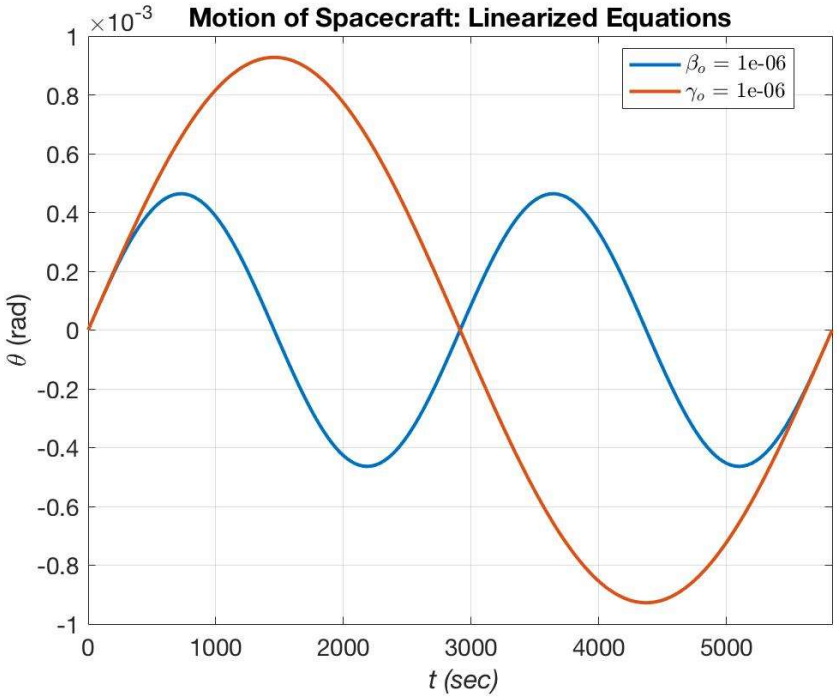


Figure 15. Numerical Solution to Motion Equations: $\varphi = 85°$, $\dot{\alpha}_0 = 0$

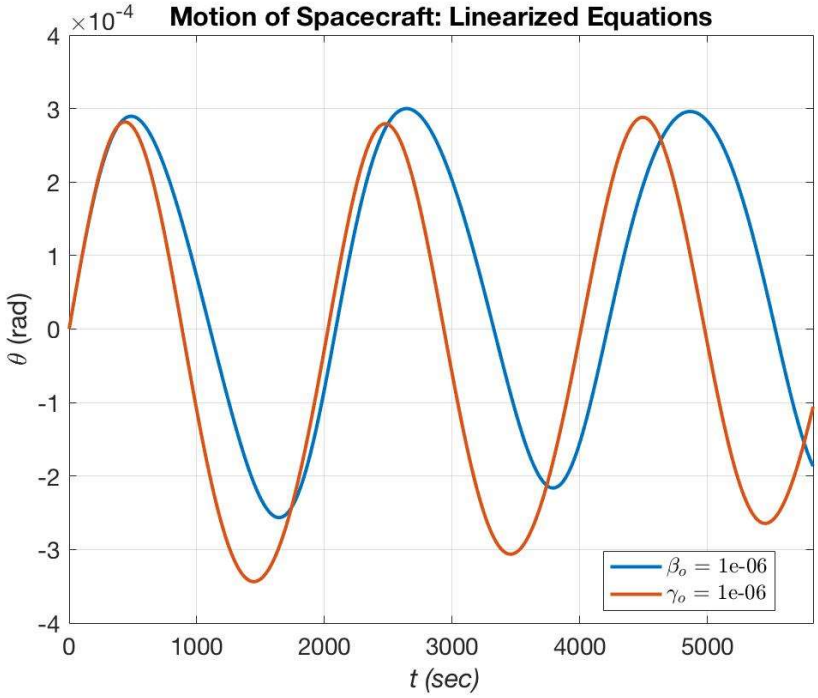


Figure 16. Numerical Solution to Motion Equations: $\varphi = 85°$, $\dot{\alpha}_0 = 2\Omega_c$

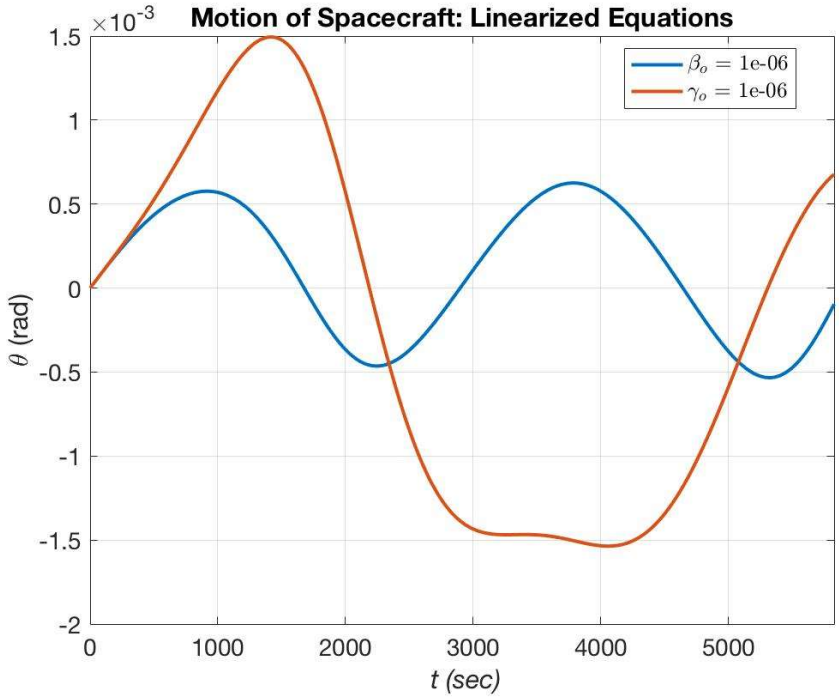


Figure 17. Numerical Solution to Motion Equations: $\varphi = 85°$, $\dot{\alpha}_0 = -\Omega_c$

Again, at first glance it appears that the results of the numerical integration for first two runs show stable motion of the TSS. For the third run, it appears that the motion of the TSS is unstable. It is common practice in spacecraft dynamics to use Floquet analysis to determine a the stability properties of a spacecraft. It requires, however, that the equations of motion are ordinary differential equations with periodic coefficients. We assume for now that the equations of motion have periodic coefficients. This assumption is validated below once we solve for $\alpha$. Therefore, we can validate these results using Floquet analysis.

Floquet analysis requires a system of ordinary differential equations with periodic coefficients. A system of two equations, using the variables from the equations of motion, is written in the form

$$\frac{d}{dt}\begin{bmatrix}\beta\\ \gamma\\ \dot{\beta}\\ \dot{\gamma}\end{bmatrix} = -\begin{bmatrix}0 & 0 & -1 & 0\\ 0 & 0 & 0 & -1\\ p(t)_{\beta\beta} & p(t)_{\beta\gamma} & 0 & 0\\ p(t)_{\gamma\beta} & p(t)_{\gamma\gamma} & 0 & 0\end{bmatrix}\begin{bmatrix}\beta\\ \gamma\\ \dot{\beta}\\ \dot{\gamma}\end{bmatrix} \tag{42}$$

where $p(t)_{ij}$ terms are all periodic (e.g., sin and cos). The *i* and *j* indices correspond to the equations of motion for $\ddot{\beta}$ and $\ddot{\gamma}$, and periodic coefficients for the $\beta$ and $\gamma$ terms, respectively. We then numerically integrate the series of equations from $t = 0$ to $t = T$. Equations 40 and 41 that describe the motion of the triangle TSS, however, are not in a form that can be used in a Floquet analysis. We need to determine a solution to the in-plane rotation motion (i.e., $\alpha$), which is in the form of a periodic elliptic function, to perform the analysis. Finding the solution to $\alpha$ requires us to solve for the energy integral associated with $\alpha$, which we can determine by integrating Equation 37. After integration, the energy integral for the system is

$$\dot{\alpha}^2 + 3\Omega_c^2 k_2 \, \mathrm{s}^2 \, \alpha = a^2 = \text{constant} \tag{43}$$

where $a$ is determined by the initial conditions. We know from Hughes that the solution to Equation 43 is in the form of a Jacobi elliptic function [9]. These functions are commonly used to describe the motion of a pendulum. Assuming $\alpha(0) = 0$, the solution for the energy equation is as follows

$$\sin\alpha = \begin{cases}\hat{a}\,\mathrm{sn}\left(\dfrac{at}{\hat{a}};\hat{a}\right) & (0 < \hat{a} < 1)\\ \mathrm{sn}(at;\hat{a}^{-1}) & (\hat{a} \geq 1)\end{cases} \tag{44}$$

where $a$ is defined as

$$a = |\dot{\alpha}(0)| \tag{45}$$

and $\hat{a}$ is defined as:

$$\hat{a} = \frac{a}{\sqrt{3k_2}\Omega_c} \tag{46}$$

The period over which we will solve the differential equation is

$$T = \begin{cases} 4K(\hat{a}) & (0 < \hat{a} < 1) \\ \dfrac{4K(\hat{a}^{-1})}{a} & (\hat{a} \geq 1) \end{cases} \tag{47}$$

which aligns the period of the circular orbit to that of the Jacobi elliptic function. Additionally, we need four sets of linearly independent initial conditions for the equations. The initial conditions used are shown in Equation 48:

$$\begin{bmatrix} \beta \\ \gamma \\ \dot{\beta} \\ \dot{\gamma} \end{bmatrix} = \begin{bmatrix} 1 \\ 0 \\ 0 \\ 0 \end{bmatrix}, \begin{bmatrix} 0 \\ 1 \\ 0 \\ 0 \end{bmatrix}, \begin{bmatrix} 0 \\ 0 \\ 1 \\ 0 \end{bmatrix}, \begin{bmatrix} 0 \\ 0 \\ 0 \\ 1 \end{bmatrix} \tag{48}$$

Finally, the last equation that we define for the analysis is a non-dimensional term, initially chosen by Kane and Shippy and used by Hughes [9], for the "average relative spin rate" of the TSS:

$$s \triangleq \frac{\overline{\dot{\alpha}}}{\Omega_c} \equiv (\pm)\frac{2\pi}{\Omega_c T} \tag{49}$$

With the values for the initial conditions and $s$ identified, we can conduct the Floquet analysis to determine the stability of the triangle TSS. The results of the Floquet analysis are presented next in Chapter 4.

In this chapter, we accomplished several of the steps needed to analyze the stability of a triangle TSS. First step was deriving the nonlinear equations of motion for a spinning triangle TSS, shown in Equations 29-31. Second step was solving the nonlinear equations using two sets of initial equations in order to determine a point around which the spinning

spacecraft motion is stable ($\dot{\beta} = \beta = 0$ and $\dot{\gamma} = \gamma = 0$). Third step was linearizing the motion equations around the point of known stable motion as shown in Equations 40-41. Finally, we found a solution to the equation for $\alpha$, which was periodic in nature. Thus, we can apply Floquet analysis to determine the stability of our system since the resulting differential equations that describe the spacecraft motion have linear periodic coefficients. The setup for the Floquet analysis is outlined above. The results of the Floquet analysis are shown in Chapter 4 Results.

# Chapter 4

## Results

This chapter presents the results of the analysis performed in Chapter 3. The numerical integration of Equations 37, 40, and 41 uses the initial conditions from Equation 48 and is performed for $60° \leq \varphi < 90°$ at increments of 1°, and $-3 \leq s \leq 3$ at increments of 0.1. The individual spacecraft have mass of 1 kg (3 kg total). The tether length 'a', as defined in Figure 9, is set at 10 km. The central mass around which the triangle TSS is orbiting is the Earth ($\mu = 3.986 \times 10^5$ km$^2$/s$^2$, and $r = 6374$ km), and the TSS orbits at an altitude of 626 km ($r_c = 6374$ km). The initial condition for the orientation of the triangle TSS is $\alpha = 0°$. The initial values listed above are the complete set of conditions used to set up the triangle TSS for analysis.

## Review of Model Results

A summary of the results obtained from the Floquet analysis are shown below in Figure 18. A select set of $\varphi$ and the respective values of $k_2$ used in the analysis are shown in Table 5. The values of $k_1$ and $k_3$ are not shown because they are always equal to one, with one exception.

Table 5. Value of $k_2$ as a Function of $\varphi$ for Triangle TSS

| $\varphi$ (deg) | $k_2$ |
|---|---|
| 60 | 0.000 |
| 65 | 0.213 |
| 70 | 0.442 |
| 75 | 0.666 |
| 80 | 0.851 |
| 85 | 0.965 |
| 90 | 1.000 |

That exception is one of two edge cases for $k$ worth noting. The first is the cases of $\varphi = 60°$, where $k_2 = 0$, and the second is at $\varphi = 90°$, where $k_3 = \infty$. No results were obtained for $\varphi = 90°$ due to the singularity that occurs at that point. This is the case for a rod with two masses, one at each end of the rod.

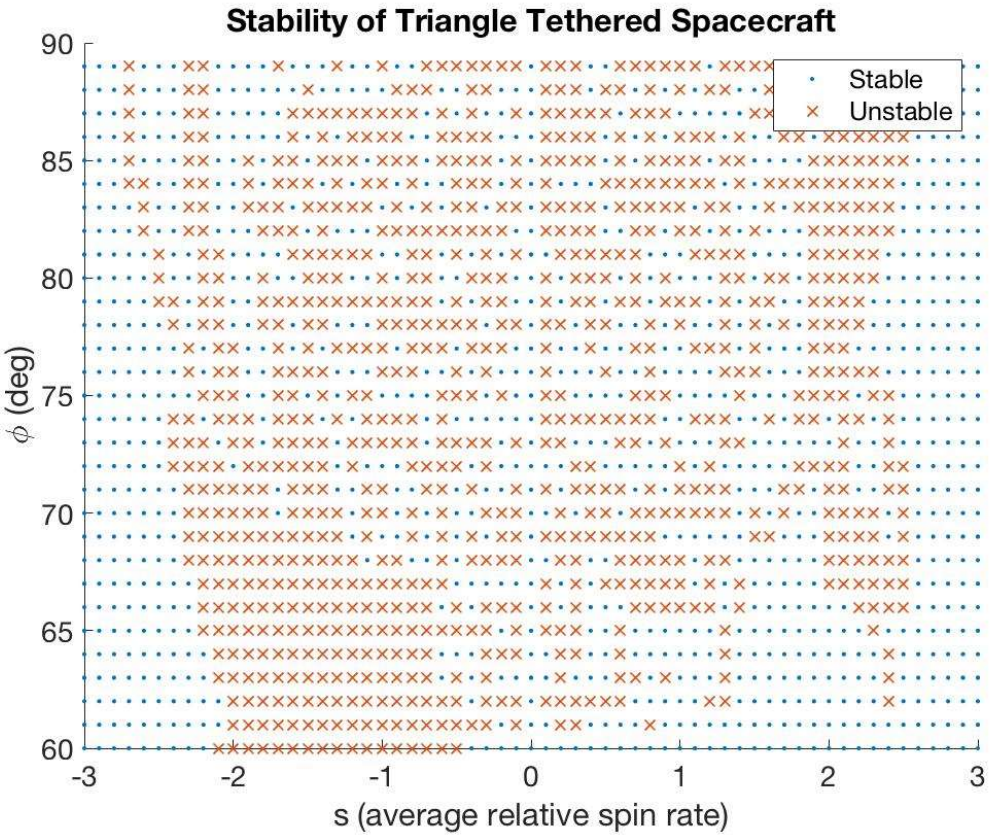


Figure 18. Floquet Analysis Results for Triangle TSS: $\varphi$ vs $s$

For the case of $\varphi = 60°$, we have an equilateral triangle and an axisymmetric rigid body. The equilateral triangle case reduces the equations of motion to a form no longer in need of Floquet analysis to determine the stability. We are still, however, able to analyze stability of the axisymmetric case, as we can see above in Figure 18. Further analysis of this special case was performed by Hughes [9] and we do not repeat his work here. For the case of $\varphi = 90°$, we end up at the case of a dumbbell satellite. This specific case was studied by Ellis and again we do not repeat his work here [8]. Another case worth exploring is the case of $s = 0$, where the satellite is not spinning with respect to the orbital frame. In this case, the triangle TSS is stable for all values of $\varphi$. The $s = 0$ case is the same as the case of an Earth-pointing satellite in a circular orbit, which Hughes and others previously analyzed [9]. We refer to Figure 18 for the remaining cases of $\varphi$ and $s$ to determine the stability of the triangle TSS. The main takeaway from Figure 18 is that there is a clear band of instability. Between $-2.8 < s < 2.6$, stability can change quickly as the spin rate and geometry of the triangle TSS change. At many points, $\pm 1°$ of $\varphi$ or $\pm 0.1$ of $s$ can make the difference between a stable system and an unstable system. For this reason, it is recommended that an operational system of this nature spin at a relative rate of approximately $\pm 3$ times the rate at which it is orbiting the Earth. If we run a more closely spaced mesh at the stability boundaries, however, we get a much clearer picture of the conditions that cause the triangle TSS to become unstable. The following two figures are created using an increment of $0.1°$ for $\varphi$ and $0.01$ for $s$. Figure 19 shows the region between $-3 < s < -2$, and Figure 20 shows the region between $2 < s < 3$.

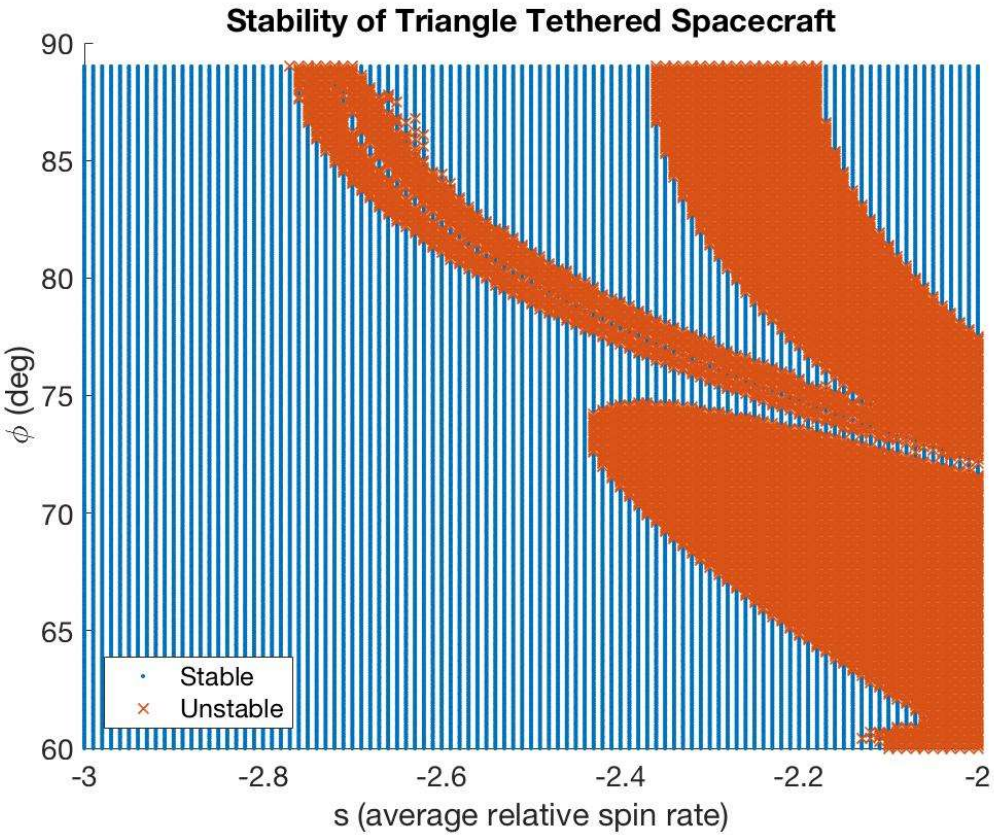


Figure 19. Close Up of Floquet Analysis Results for $-3 < s < -2$

These figures clearly delineate between regions of stability and instability for the triangle TSS. The additional detail afforded by the more closely space mesh shows detail that was lost in the coarse mesh of Figure 18. One example is the thin band of stability shown within a region of instability that was not shown before. While the closely spaced mesh does allow for additional fidelity, it is still recommended that a triangle TSS is not operated within that narrow stability band as it does not provide much margin for error or to change the spin rate post deployment.

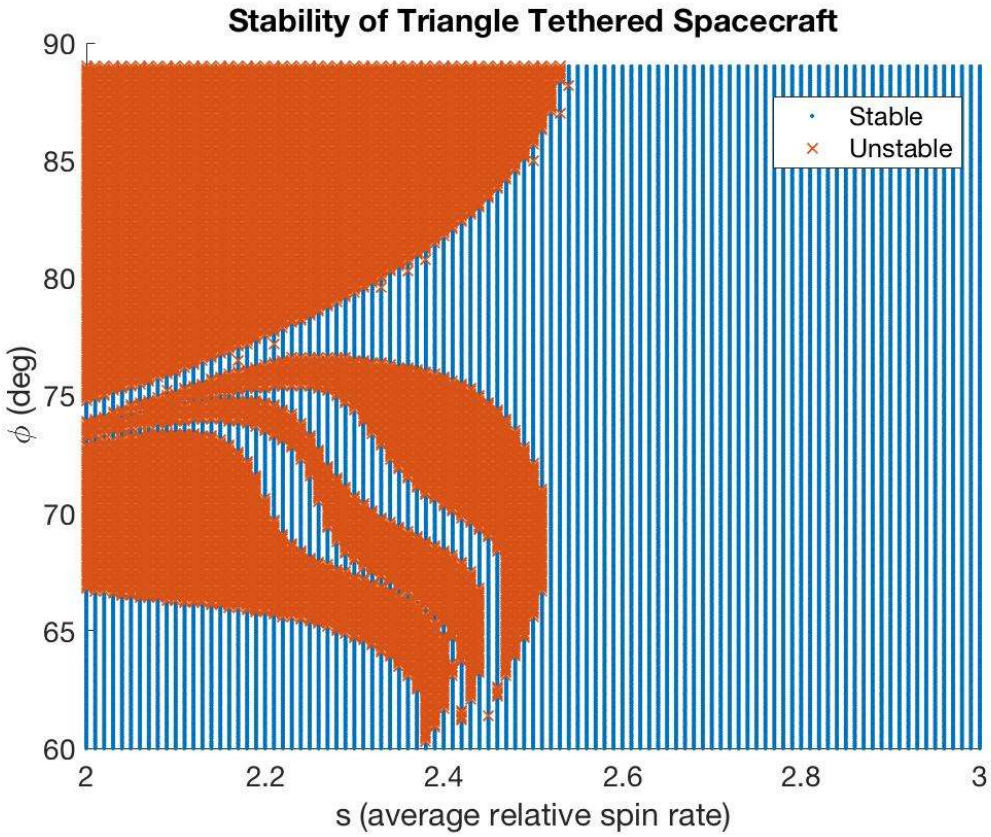


Figure 20. Close Up of Floquet Analysis Results for $2 < s < 3$

We can now validate the stability predictions made in Chapter 3 using the results of the Floquet analysis. For Test Case 1 ($\varphi = 70°$), we predicted the stability properties as stable, stable, and unstable for $\dot{\alpha}_0 = 0$, $\dot{\alpha}_0 = 2\Omega_c$ , and $\dot{\alpha}_0 = -\Omega_c$, respectively. Looking at the results in Figure 18, we can see that the predicted stability in one case does not matches the results of the Floquet analysis. The system is unstable for the case of $\dot{\alpha}_0 = 2\Omega_c$. For Test Case 2 ($\varphi = 85°$), we also predicted that the stability properties as stable, stable, and unstable for $\dot{\alpha}_0 = 0$, $\dot{\alpha}_0 = 2\Omega_c$ , and $\dot{\alpha}_0 = -\Omega_c$, respectively. Looking at the results in Figure 18, we can see that the predicted stability for one case again does not match the Floquet analysis. The system is unstable at $\dot{\alpha}_0 = 2\Omega_c$. It appears that it is

possible to make predictions about the stability from the results of numerical analysis alone. However, it is not recommended given the unstable nature of system behavior and the likelihood for error, as demonstrated above. Floquet analysis is the recommended approach to determine stability of a spinning TSS.

# Chapter 5

## Summary and Recommendations for Future Work

The stability analysis performed in this thesis and presented in the Results chapter is for a specific set of conditions. These conditions include representing the TSS as a rigid body; constraining the TSS to an unperturbed circular orbit with only gravity gradient torque acting on the system; and assuming that the out-of-plane angles $\beta$ and $\gamma$ remain small. This results in a situation where the TSS remains stable for all geometric configurations when the relative spin rate is $-2.8 < s < 2.6$. There are several ways in which we can change the assumptions made in this analysis to provide additional constraints to the analysis of a triangle TSS.

## Summary of Contributions

The Floquet analysis conducted in Chapter 4 calculated the stability conditions for a spinning triangle TSS as a function of the average relative spin rate *s*, and $\varphi$. The results of the analysis were presented in graphical form showing stability for a spinning triangle TSS. That graph is the central contribution of this thesis. This graph shows that for $-2.8 < s < 2.6$, we can assume stable motion regardless of $\varphi$ for the triangle TSS. The work to comprehensively analyze the stability of a triangular rigid body was the first performed to date. This work also confirmed the derivation of the motion equations, both nonlinear and linear, for a spinning tri-inertial rigid body using a different a different set of rotations than Hughes. The linearized, periodic coefficient, form of the equations of motion were required for the Floquet analysis to determine stability of a rigid-body.

## Recommendations for Future Work

There are several options available to expand upon the work performed in this thesis. The first would be to loosen the assumption that we treat the triangle TSS as a rigid body. This would require first analyzing cases in which the combinations of triangle geometry and relative spin rate cause the tether to go slack. This would further constrain stability results only the combinations of geometric shape and spin rate where the tether remain taut. There are existing equations for tension in a spinning tethered spacecraft that we can leverage for this purpose. Second, the work could expand upon the triangle assumption and look at additional tether spacecraft formations, which would greatly expand the TSS formations for which the governing equations of motion are known. Third, we could assume the tether is conducting and consider the effects of additional perturbations (e.g., electrodynamic forces, drag) on stability. Finally, a future analysis could look at stability properties for an elliptical orbit instead of a circular orbit. All of these recommendations are areas in which one could expand upon the work performed in this thesis.

## References


[1] V. S. Aslanov and A. S. Ledkov, Dynamics of tethered satellite systems, Philadelphia: Woodhead Publishing, 2012.

[2] M. L. Cosmo and E. C. Lorenzini, Eds., *Tethers in Space Handbook, Third Edition,* Washington, D.C.: NASA, 1997.

[3] Naval Research Laboratory, "Tether Physics and Survivability Experiment (TiPS)," U.S. Navy, [Online]. Available: https://www.nrl.navy.mil/ssdd/programs/tips. [Accessed 29 Oct 2017].

[4] V. V. Beletsky and E. M. Levin, Dynamics of Space Tether Systems, San Diego: American Astronautical Society, 1993.

[5] Y. Chen, R. Huang, L. He, X. Ren and B. Zheng, "Dynamical modelling and control of space tethers: a review of space tether research," *Nonlinear Dynamics,* vol. 77, no. 4, pp. 1077-1099, 2014.

[6] M. Kim and C. D. Hall, "Control of a Rotating Variable-Length Tethered System," *Journal of Guidance, Control, and Dynamics,* vol. 27, no. 5, pp. 849-858, 2004.

[7] C. D. Hall and J. R. Ellis, "Out-of-plane librations of spinning tethered satellite systems," *Celestial Mechanics and Dynamical Astronomy,* vol. 106, pp. 39-67, 2010.

[8] J. R. Ellis, *Modeling, Dynamics, and Control of Tethered Satellite Systems,* Blacksburg, VA, 2011.

[9] P. C. Hughes, Spacecraft Attitude Dynamics, Mineola: Dover Publications, Inc., 2004.

[10] T. M. Berman, "The Sentinel: Mission Analysis, Dynamics & Control of a Tethered-Antenna CubeSat," Virginia Polytechnic Institute & State University, Blacksburg, 2010.

[11] B. C. Hacker and J. M. Grimwood, "On The Shoulders of Titans: A History of Project Gemini," NASA, Washington, 1977.

[12] N. H. Stone, "Unique Results and Lessons Learned From the TSS Missions," in *Fifth International Conference on Tethers in Space*, Ann Arbor, 2016.

[13] J. R. Glaese, "Small Expendable Tether Deployer Systems (SEDS) Tether Dynamics Analysis," NASA Marshal Space Flight Center, Huntsville, 1996.

[14] National Reconnaissance Office, "National Reconnaissance Office Press Releases," 20 November 1996. [Online]. Available: http://www.nro.gov/news/press/1996/1996-08.pdf. [Accessed 29 October 2017].

[15] J. W. Powell, "Tether Experiment," *Spaceflight,* vol. 39, pp. 120-121, April 1997.

[16] E. J. van der Hiede and M. Kruijff, "Data Analysis of a Tethered SpaceMail Experiment," *Journal of Spacecraft and Rockets,* vol. 46, no. 6, pp. 1272-1287, 2009.

[17] European Space Agency, "YES2 Team Claims a Space Tether World Record," European Space Agency, 8 November 2007. [Online]. Available: http://www.esa.int/Education/Young_Engineers_Satellites/. [Accessed 29 October 2017].

[18] E. C. Lorenzini, "The Propulsive Small Expendable Deployer System Final Report," NASA, Huntsville, 2003.

[19] N. P. Hansen, L. S. Marshall, W. B. Lytle, F. M. Kustas and B. McCandless II, "Design Concept for a Reusable/Propellantless MXER Tether Space Transportation System," in *53rd JANNAF Propulsion Meeting*, Montery, 2005.

[20] D. A. Quinn and D. C. Folta, "A Tethered Formation Flying Concept for the SPECS Mission," in *Guidance and Control Conference*, Breckenridge, 2000.

[21] C. D. Hall and M. Kim, "Dynamics and Control of Rotating Tethered Satellite Systems," *Journal of Spacecraft and Rockets,* vol. 44, no. 3, pp. 649-659, 2007.

[22] E. Topal and U. Daybelge, "Dynamics of a Triagular Tethered Satellite System on a Low Earth Orbit," in *Proceedings of the 2nd International Conference on Recent Advances in Space Technologies*, Istanbul, 2005.

[23] C. D. Hall, Spacecraft Attitude Dynamics and Control, 2010.

[24] E. M. Levin, Dynamic Analysis of Space Tether Missions, San Diego: Univelt Incorporated, 2007.